Journal of Materials Chemistry A

Low-Temperature Solution-Grown $CsPbBr_3$ Single Crystals and Their Characterization

Journal:	*Journal of Materials Chemistry A*
Manuscript ID	Draft
Article Type:	Paper
Date Submitted by the Author:	n/a

Complete List of Authors:	Rakita, Yevgeny; Weizmann Institute of Science, Materials and Interfaces Kedem, Nir; Weizmann Institute of Science, Materials and Interfaces Gupta, Satyajit; Weizmann Institue of Science, Materials and Interfaces Sadhanala, Aditya; University of Cambridge, Department of Physics, Cavendish Laboratory Kalchenko, Vyacheslav; Weizmann Institute of Science, Materials and Interfaces Böhm, Marcus; University of Cambridge, Cavendish Laboratory Kulbak, Michael; Weizmann Institute of Science, Materials and Interfaces Friend, Richard; Optoelectronics Group, Cavendish Laboratory Cahen, David; weizmann institute, materials and interfaces Hodes, Gary; Weizmann Inst, Materials and Interfaces

Cover Letter for ms. on

Low-Temperature Solution-Grown $CsPbBr_3$ Single Crystals and Their Characterization

Authors:

Mr. Yevgeny Rakita
Dr. Aditya Sadhanala
Mr. Michael Kulbak
Prof. Gary Hodes
Dr. Nir Kedem
Dr. Vyacheslav Klachenko
Prof. Richard H. Friend
Dr. Satyajit Gupta
Dr. Marcus L. Böhm
Prof. David Cahen

Corresponding Authors:

Prof. Gary Hodes
Dept. of Materials and Interfaces
Weizmann Institute of Science
Rehovot, Israel 76100
+972-8-934-2246
Gary.Hodes@weizmann.ac.il

Prof. David Cahen
Dept. of Materials and Interfaces
Weizmann Institute of Science
Rehovot, Israel 76100
+972-8-934-2246
david.cahen@weizmann.ac.il

Manuscript Type:

Article

Submitted to:

Journal of Materials Chemistry A

Manuscript Significance:

Dear Editor,

The tremendous success of halide perovskites (AMX_3) in optoelectronic and especially, photovoltaic applications stimulates efforts to elucidate fundamental physicochemical properties of these materials.

Many of these efforts require insight into the bulk and surface properties of these materials, where a well-defined system, such as a *single crystal*, is necessary. Indeed, in recent years single crystals of these materials have come to the forefront as materials for experiments.

At the same time, there is increasing interest in *all-inorganic halide perovskite $CsPbBr_3$-based* optoelectronic devices, because of significantly improved stability over that possible with organic-inorganic hybrids and because of intrinsic interest to understand the role of the organic moiety in the properties of these halide perovskites.

Until now, $CsPbBr_3$ single crystals were grown under conditions that were quite different (including > 600 °C using the Bridgman method) from those used to prepare films for device work, as for the latter *organic solvent-based methods* are used.

In this manuscript we describe, for the first time, *two* approaches to grow, in a matter of hours to few days, mm-size $CsPbBr_3$ high quality single crystals:

(1) anti-solvent-vapor saturation and

(2) heating a solution containing retrograde soluble $CsPbBr_3$.

Both are methods that are already used for the growth of hybrid organic-inorganic halide perovskites, which imparts added value to the methods that we report here. This is because it should be possible for those interested, to adapt the methods for the growth of crystals with mixed occupation of the A site, buy both an inorganic and organic cation. The importance of that is underscored by recent publications that use films of such materials.

Because of this last aspect and so as not to follow the often-times sketchy descriptions given in publications in this field, we go into great detail in our description of the procedures to allow other research groups to reproduce our results. We also show how to avoid the commonly present CsBr-rich (Cs_4PbBr_6) or $PbBr_2$-rich ($CsPb_2Br_5$) phases, and to growth pure $CsPbBr_3$ crystals. We provide several characterizations to assess the potential of these solution-grown crystals for optoelectronics and photovoltaics, including first results of charge carrier lifetime and of the Urbach energy.

We hope that this contribution will be on interest to the readers of J. Mater. Chem. A.

Sincerely,

Gary Hodes and David Cahen

208x159mm (300 x 300 DPI)

Low-Temperature Solution-Grown $CsPbBr_3$ Single Crystals and Their Characterization

Yevgeny Rakita[a], Nir Kedem[a], Satyajit Gupta[a], Aditya Sadhanala[b], Vyacheslav Kalchenko[c], Marcus L. Böhm[b], Michael Kulbak[a], Richard H. Friend[b], David Cahen[a]* and Gary Hodes[a]*

a. *Materials and Interfaces Department, Weizmann Institute of Science, Rehovot, 7610001, Israel*
b. *Cavendish Laboratory, JJ Thomson Avenue, Cambridge CB3 0HE, United Kingdom*
c. *Veterinary Resources Departments; Weizmann Institute of Science, Rehovot, 7610001, Israel*

* Corresponding authors: Gary Hodes: gary.hodes@weizmann.ac.il ; David Cahen: david.cahen@weizmann.ac.il

Keywords: Halide Perovskite, Single Crystal, Photovoltaics, Urbach energy

Abstract:

Cesium lead bromide ($CsPbBr_3$) was recently introduced as a potentially high performance thin-film halide perovskite (HaP) material for optoelectronics, including photovoltaics, significantly more stable than $MAPbBr_3$ ($MA=CH_3NH_3^+$). Because of the importance of single crystals to study relevant material properties *per se*, crystals grown under conditions comparable to those used for preparing thin films, i.e. *low-temperature solution-based* growth, are needed. We show here two simple ways: anti-solvent-vapor saturation or heating a solution containing retrograde soluble $CsPbBr_3$, to grow single crystals of $CsPbBr_3$ from a precursor-solution, treated with acetonitrile (MeCN) or methanol (MeOH). The precursor solutions are stable for at least several months. Millimeter-sized crystals are grown without crystal-seeding and can provide a 100% yield of $CsPbBr_3$ perovskite crystals, avoiding a CsBr-rich (or $PbBr_2$-rich) composition, which is often present along-side the perovskite phase. Further growth has been demonstrated to be possible with crystal-seeding. The crystals are characterized in several ways, including first results of charge carrier lifetime (30 ns) and an upper-limit of the Urbach energy (19 meV). As the crystals are grown from a polar solvent (DMSO), which is similar to those used to grow hybrid organic-inorganic HaP crystals, this may allow growing mixed (organic and inorganic) monovalent cation HaP crystals.

Introduction:

In the last few years, halide perovskites (HaPs) with AMX_3 stoichiometry (where *A* is methylammonium (MA), formamidinium (FA) or cesium (Cs) ; *M*=Pb or Sn ; *X*=Cl, Br, I) have attracted attention because of their remarkable optoelectronic (especially photovoltaic) properties, compared to other competitive, low-cost, optoelectronic materials (e.g., various organic molecules and polymers, CdX, PbX (X=S, Se, Te), $Cu(In,Ga)Se_2$).[1,2] Some compositions of AMX_3 yield small area photovoltaic light-to-electrical conversion efficiencies above 21%[2], and also relatively efficient and tunable light-emitting diodes[3,4], photodetectors/resistors[5,6] and high-energy radiation detectors[7]. To help understand the remarkable optoelectronic properties of these materials, one would like to be able to study bulk material of controlled quality, prepared under conditions that are not too different from those used for making films employed in most HaP-based devices. Clearly single crystals are a desirable form of materials for this purpose.

$CsPbBr_3$,[8,9] has recently gained attention as a stable HaP, but hitherto no method was available to prepare macroscopic crystals by the low temperature solution methods that are used to make films for photovoltaic cells. For the hybrid organic–inorganic halide perovskites (where A is usually MA or FA), it was already demonstrated that single crystals with mm to cm dimensions can be grown using different solution-based methods at low-temperature (around or below 100°C): anti-solvent vapor saturation[10,11], slow heating of a solution with a retrograde-soluble compound[12], or top-seeded slow-cooling in a precursor-solution.[13,14] However, organic elements in these compositions can act as 'weak links' and decrease the stability (and thus reliability) of the entire structure, as was demonstrated in a comparison between the $MAPbBr_3$ and $CsPbBr_3$ HaPs.[8] It was also shown that exchanging to the fully inorganic compound (i.e. $CsPbBr_3$) does not necessarily exact a price in photovoltaic performance.[9] To be able to use single crystals to study $CsPbBr_3$ and compare it with its organic-inorganic hybrid analogs, the single crystals should preferably be prepared under conditions that are comparable to those of the thin films used in device work. While the hybrid HaPs can indeed be grown from solution, no such process was available for $CsPbBr_3$. Here we report on this missing link.

At standard temperature and pressure, the perovskite-like structure is the thermodynamically most-stable structure of $CsPbCl_3$ and $CsPbBr_3$ (but not of $CsPbI_3$).[15] The only reported procedure of making mm-size single crystals of these materials is by Bridgman

growth[7,16], where precursors are melted (above 600°C) in a quartz tube and passed through a multi-temperature zone tube furnace).

For hybrid organic-inorganic perovskites the known compositions that can be created have a single stoichiometric composition (i.e. AMX_3) regardless of precursor ratio and present a retrograde-solubility in a variety of organic solvents[17], which allow an efficient and easy single-crystal growth. For the fully inorganic analog (for our particular interest: $CsPbBr_3$), on the other hand, the situation is more challenging. First, similar to compositions with other alkaline *A* atoms, such as RbBr:$PbBr_2$, in the CsBr:$PbBr_2$ system 1:2 and 4:1 compositions, as well as the 1:1 perovskite one, are known.[18] Furthermore, there is a large difference in the solubility of $PbBr_2$ and CsBr in aprotic solvents. Usually, CsBr is less soluble than $PbBr_2$ in aprotic solvents like dimethylformamide, gamma-butyrolactone, dimethylsulfoxide (generally used for growing hybrid-halide perovskites single crystals) and CsBr-rich products (e.g., CsBr:$PbBr_2$ = 4:1; Cs_4PbBr_6) tend to form. Thus, growing material with the 1:1 ($CsPbBr_3$) composition presents a serious challenge.

Although Cs_4PbBr_6, was usually evident as the main or side product, we found conditions that allow growth of pure $CsPbBr_3$ crystals, without the presence of additional phases. Two low-temperature (< 100ºC, down to room-temperature) methods were used:

-1- slow anti-solvent vapor saturation of a precursor solution and

-2- slow heating of a solution containing $CsPbBr_3$ as a retrograde-soluble compound.

Here we describe the procedures to grow $CsPbBr_3$ crystals with dimensions of several mm from a precursor solution. The precursor solution was found to be stable for several months, and larger crystals (using $CsPbBr_3$ crystal seeds) could be further grown with it. We provide several characterizations to assess the potential of these solution-grown crystals for optoelectronics and photovoltaics, including first results of charge carrier lifetime and of the Urbach energy.

Protocol for crystal growth

Precursors

Powders of cesium bromide (CsBr) (Aldrich, 99.999%) without further purification and lead bromide ($PbBr_2$) (Aldrich, ≥98%) that was dried in a vacuum oven overnight, were dissolved in dimethylsulfoxide (DMSO) (Aldrich, ≥99.9%). Acetonitrile (MeCN) (BioLab LTD, HPLC grade, 99.97%) and methanol (MeOH) (BioLab LTD, HPLC grade, 99.95%) were used as received.

Precursor Solution preparation

A 0.45 M solution (slightly below the ~ 0.5 M solubility limit) of the perovskite precursors (equimolar amounts of CsBr and $PbBr_2$) in the same solution of DMSO was prepared in ambient air (ca. 45% RH) under continuous stirring at ~50^{o}C, until no powder is observed. It is important to mix the precursors in the same volume, because the room temperature solubility limit of CsBr in DMSO is ca. 0.25 M when it is dissolved separately. After cooling to room temperature, the DMSO solution was titrated (dropwise under continuous stirring) with MeCN or MeOH. During the titration, a yellow-orange precipitant appeared with addition of each drop and quickly re-dissolved. As the system gets closer to the saturation point (more pronounced when MeCN is added), a permanent white solid precipitates (*Fig. S1(a)*). At MeCN : DMSO and MeOH : DMSO ratios of 1.1 : 1 and 0.55 : 1, respectively, the yellow-orange precipitate no longer re-dissolved. These saturated solutions were thoroughly sealed (to prevent loss of the volatile MeCN or MeOH) and stirred for 24 hours at 50 °C. After heating for 24 h, a pale green-yellow strongly-fluorescent precipitant was clearly observed along-side the other precipitated species (*Fig. S1(b)*). The saturated solutions can be further stored (best in the dark) for at least several months, until their use for crystal growth. Before crystal growth, the saturated precursor solutions are filtered with PTFE 0.2 μm pore-size syringe filters. No noticeable differences in crystal growth or kinetics were observed between properly stored or freshly prepared solutions.

Crystal growth

-1- slow Vapor-Saturation of an Anti-solvent (VSA)

The concept of slow saturation with the vapor of an anti-solvent was shown earlier to be a possible method to grow different hybrid organic-inorganic HaPs.[10,11] A scheme of the crystallization setup is presented in *Fig. S2(a).* The filtered precursor solutions were placed in a clean crystallization flask and covered with a filter paper and a glass petri-dish on top to limit anti-solvent vapor diffusion. The covered crystallization flask was then placed inside a deeper, flat-bottomed, glass dish, which contained MeCN or MeOH (anti-solvent). The anti-solvent was chosen to be similar to the one previously used for saturating (titrating) the DMSO precursor-solution. Sealing the outer glass flask was done using a filter paper and glass top. In this case, the filter paper was used to create balanced anti-solvent atmosphere and to prevent the anti-solvent from condensing and dripping on the crystallization inner-setup. While crystal formation can occur at room temperature, heating the anti-solvent bath (to allow a higher anti-solvent residual vapor pressure) will accelerate the crystal growth. This can be done by placing the crystallization setup on a hot plate with the addition of an elevating element for the inner crystallization flask to minimize a non-uniform heat dissipation coming from the interface with the hot-plate.

We note that H_2O can also be used as an anti-solvent to grow $CsPbBr_3$ crystals. However, using H_2O causes the orange crystals to bleach if the amount of the anti-solvent is not carefully controlled (see *Fig. S3*). For that reason, crystals that were grown by using H_2O as an anti-solvent were not further investigated.

Fig. 1(a) shows the results of crystal growth from MeCN- and MeOH- saturated solutions. A 48 hour growth from MeCN-saturated solution showed well-faceted rectangular prisms (**Fig. 1(a,i))**, while those grown from MeOH showed a terrace-looking morphology (**Fig. 1(a,ii))**. If the same procedure is performed without the pre-saturation step, pale-yellow and strongly fluorescent precipitant, relates to Cs_4PbBr_6,[19] appear, followed by growth of $CsPbBr_3$ orange crystals on top of the Cs_4PbBr_6 crystallites (**Fig. 1(a,iii)**).

-2- Slow Heating of a solution with a Retrograde-Soluble compound (HRS)

The slow heating of a solution with a retrograde-soluble (HRS) concept was demonstrated before as an additional method to grow different hybrid organic-inorganic HaPs.[5,17,20] To grow $CsPbBr_3$ crystals the procedure is as follows: clean 4 mL or 20 mL glass vials were filled with filtered precursor-solutions and heated to the desired temperature. An unsaturated DMSO precursor-solution showed no retrograde-soluble compounds. When saturated with MeCN, and especially, with MeOH, retrograde-soluble compounds (mainly, but not only, $CsPbBr_3$) appear upon heating. To eliminate the appearance of undesirable precipitants (mostly the strongly yellow-green fluorescing Cs_4PbBr_6) a two-step heating cycle was required. First, the solution was heated to the desired temperature for 4 h and left to cool to room-temperature under continuous stirring. After all the orange precipitant dissolved, a mixture of Cs_4PbBr_6 and some unknown white precipitate was still present at the bottom of the flask. The solution was then filtered and placed in a new vial. The second heating cycle showed no additional retrograde soluble compounds apart from the orange $CsPbBr_3$ crystals (*Fig. S1(c)).* From the MeCN-saturated solution, $CsPbBr_3$ crystals start to appear clearly only above ca. 120 ºC. From the MeOH-saturated solution, however, this occurs already at ca. 40º C. To avoid crystal-growth on the sides of the glass vial, one can heat only the bottom of the vial. Due to the very low yield of crystal growth obtained from the MeCN-saturated solution, we further explored the HRS method with the MeOH-saturated solution. *Fig. S2(b)* shows a scheme of the HRS crystallization setup.

Fig. 1(b, i & ii) show $CsPbBr_3$ crystals grown from a MeOH-saturated solution with and without crystal seeding with a growth rate of 10°C /hour up to 80°C. If the same procedure is performed with only one heating cycle (**Fig. 1(b,iii)),** a strongly fluorescent CsBr-rich compound (Cs_4PbBr_6) is clearly evident together with the $CsPbBr_3$ crystals.

MeCN and MeOH were chosen from among 9 volatile commonly-used anti-solvents viz. dibromoethane, dibromomethane, ethyl acetate, 2-propanol, tetrahydrofuran, acetone, H_2O, MeCN and MeOH. All of them, except H_2O, MeCN and MeOH, showed rapid precipitation of the CsBr-rich compound, without obvious signs of $CsPbBr_3$ orange crystal growth. Therefore, they were not further investigated. Details about the different anti-solvents that did not yield CsPbBr3 crystals from DMSO solution (and for H_2O) can be found in the last section of the *Supplementary Information*.

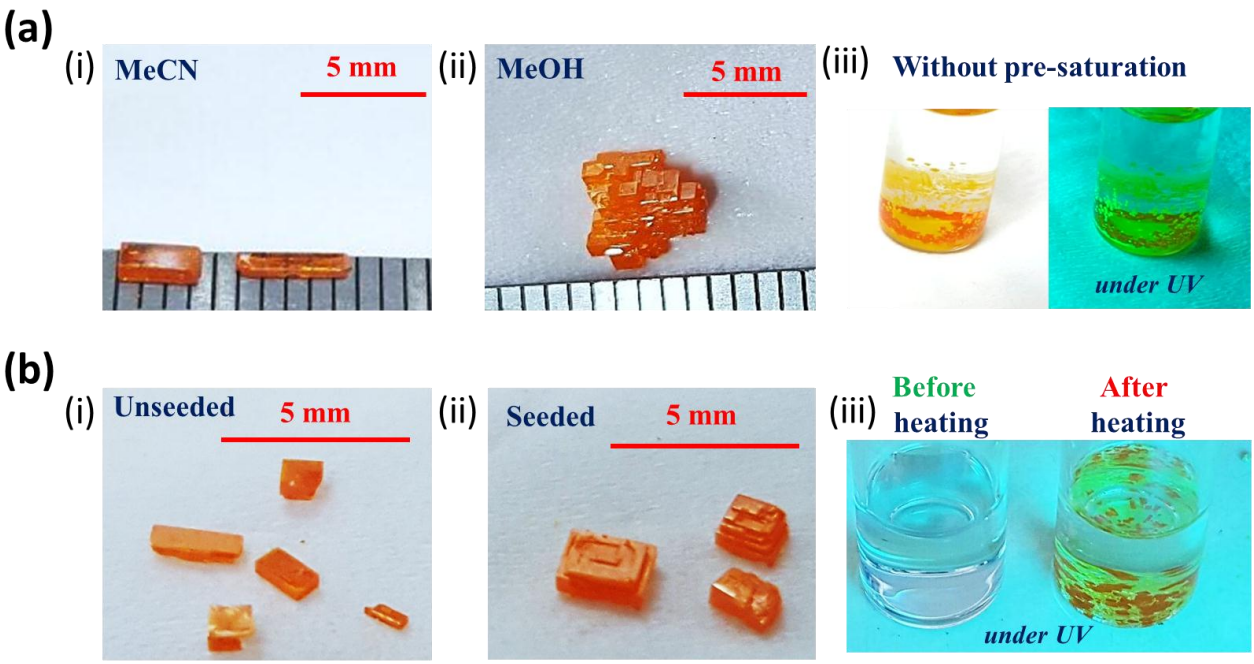

Fig. 1: (a) $CsPbBr_3$ crystals grown by a VSA method: (i) growth from MeCN-saturated solution on a 50ºC hot-plate ; (ii) growth from MeOH-saturated solutions at RT. Both were grown for ca. 48 hours; (iii) growth from an unsaturated DMSO precursor solution, using MeCN as an anti-solvent – showing (LEFT) a yellow precipitate on top of which grew orange $CsPbBr_3$. When illuminating with a UV light (RIGHT) the yellow precipitate shows a strong green fluorescence, indicating that it contains the CsBr-rich (Cs_4PbBr_6) compound. (b) $CsPbBr_3$ crystals grown by an HRS method: growth at a heating rate of 10°C/hour up to 80°C (i) without and (ii) with seeding of freshly-grown single crystals; (iii) before and after heating to 80 °C for the first time (i.e., without a preliminary heating/cooling cycle), showing the undesired Cs_4PbBr_6 fluorescent compound as a side product.

The following section deals with the characterization of the $CsPbBr_3$ crystals. Except for structural verification via XRD (**Fig. 2**) that was done for crystals grown by all the methods mentioned above, we further investigated crystals that were selected based on their (large) size and clearly developed facets. These were obtained from the VSA-growth method using a MeCN-saturated solution (as shown in **Fig. 1(a,i)**). Since seeding could induce undesirable defects at the seed boundary, we did not use crystals that resulted from seeding.

Characterization results:

For characterizing the crystals that were grown, we used:

1. powder x-ray diffraction (XRD) for structural information
2. energy-dispersive x-ray fluorescence spectroscopy (EDS) for elemental composition
3. thermogravimetric analysis (TGA) and differential scanning calorimetry (DSC) for thermal behavior (phase transition and melting point);
4. Second-harmonic generation (SHG) spectroscopy to characterize the (a-)symmetry of the crystals.
5. photothermal deflection spectroscopy (PDS), and photoluminescence spectroscopy (PL) for optoelectronic transitions (excitation and emission, respectively) and Urbach energy determination (PDS);
6. time-resolved photoluminescence (TRPL) for characterizing the lifetime of optically-excited carriers;
7. impedance spectroscopy (IS) for determining the bulk resistivity and relative permittivity, as well as measuring photo-responsivity;

Nano-indentation experiments to determine the elasto-mechanical properties of the crystals were previously reported.[21]

A brief description of the different methods can be found in a dedicated section in the *supporting information*. Whenever it was possible (based on available literature), we compared results with those of thermally grown $CsPbBr_3$ crystals.

The powder XRD spectrum of the pulverized orange crystals agrees well with that of samples obtained from melt-grown $CsPbBr_3$[7] and the simulated spectrum from a single crystal (**Fig. 2**). Placing the natively-developed face of a single crystal parallel to the scanned surface, found it to be the (101) and (002) orthogonal crystallographic planes (**Fig. 2(i)**), where (101) was found to be the more developed face. Since powder XRD might be not sensitive enough to reveal slight structural distortions, we used SHG spectroscopy to check if the solution-grown crystals retain their centrosymmetry, as expected from the *mmm* point group (orthorhombic, *Pnma* space group), to which $CsPbBr_3$ crystals were reported to belong.[7] The SHG spectroscopy was performed on a coarse-grained $CsPbBr_3$ crystal to avoid loss of signal due to phase-(mis)matching between the first and the second generated harmonics and to expose

different crystallographic orientations.[22] We observed only fluorescent emission (at 532 nm) but no SHG at half the excitation photon wavelength (Ex: 860 nm; Em: 430 nm) (**Fig. 3**). We conclude that, indeed, the crystal is centrosymmetric, agreeing with the reported crystal symmetry.

EDS yields a Cs:Pb:Br atomic ratio of (**1.00**±0.04):(**1**):(**3.4**±0.1) (taking the Pb quantity as unity). The excess in the Br signal may come from reabsorption of Pb and Cs x-ray emissions by Br (the EDS lines that were used for quantification are 1.48, 2.34 and 4.28 keV, for the Br, Pb and Cs respectively). The effect is only seen for the Br, probably as it is the most abundant element as well as its ability to absorb both the Cs and Pb x-rays. Pb, in contrast, may only absorb x-rays emitted the Cs. Based on the EDS line-spectrum (*Fig. S4*), no other elements were detected.

Thermal analysis results (**Fig. 4**) are similar to what has been reported for melt-grown $CsPbBr_3$ crystals[7,23] and to the TGA analysis of spin-coated $CsPbBr_3$[8] (i.e. tetragonal (*Pnma)* ↔ cubic (*Pm3m)* phase transformation at 131 °C [23] and melting at 567 °C [7]). The reported transition between the orthorhombic (*Pnma)* to the tetragonal (*P4/mbm*) symmetries (at 88 °C[7,23]) were not observed in our analysis, possibly due to insufficient sensitivity in the measurement. Thermal analysis performed on a single crystal (*Fig. S5*) sometime showed a sharp change (both in TGA and the first heating cycle in DSC) at ~230 °C, which may be related to trapped solvent (DMSO; bp:189 °C).

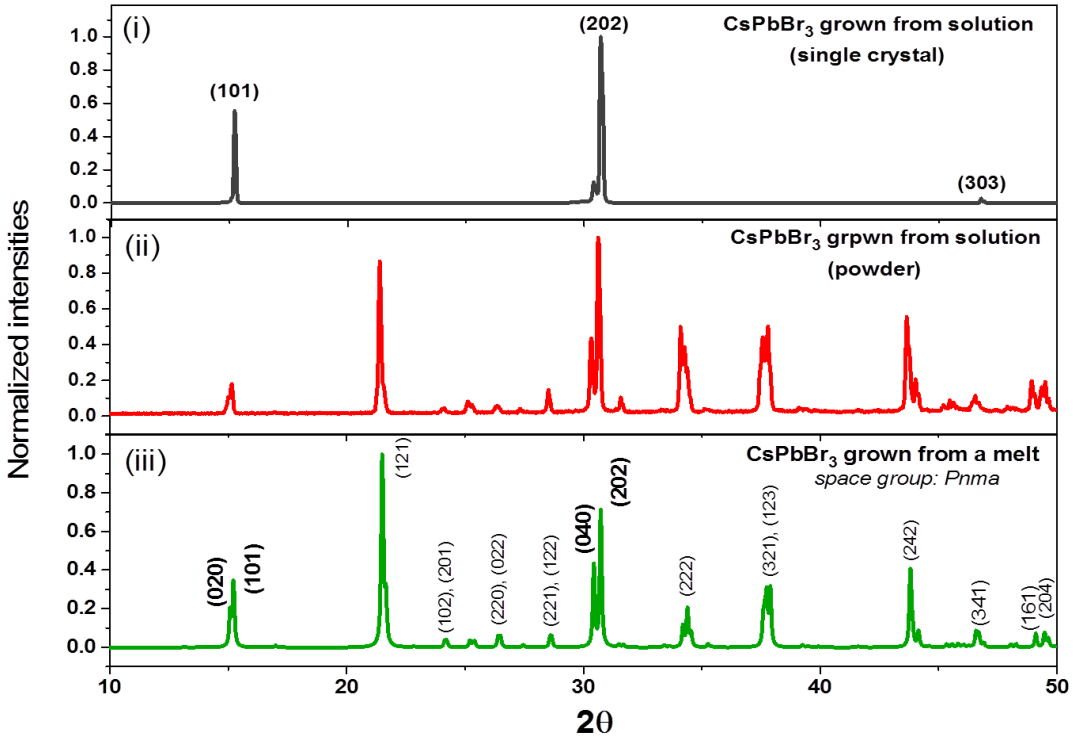

Fig. 2: Room-temperature x-ray diffraction pattern of (i) solution-grown $CsPbBr_3$ single crystal. The natively-grown face of which was parallel to the scanning plane in a θ/2θ scan; (ii) powder scan of a pulverized solution-grown single crystal and (iii) a simulated spectrum based on thermally-grown crystals' CIF.[7] The crystal orientations written in **bold** correspond to the natively-exposed faces of the solution-grown crystal.

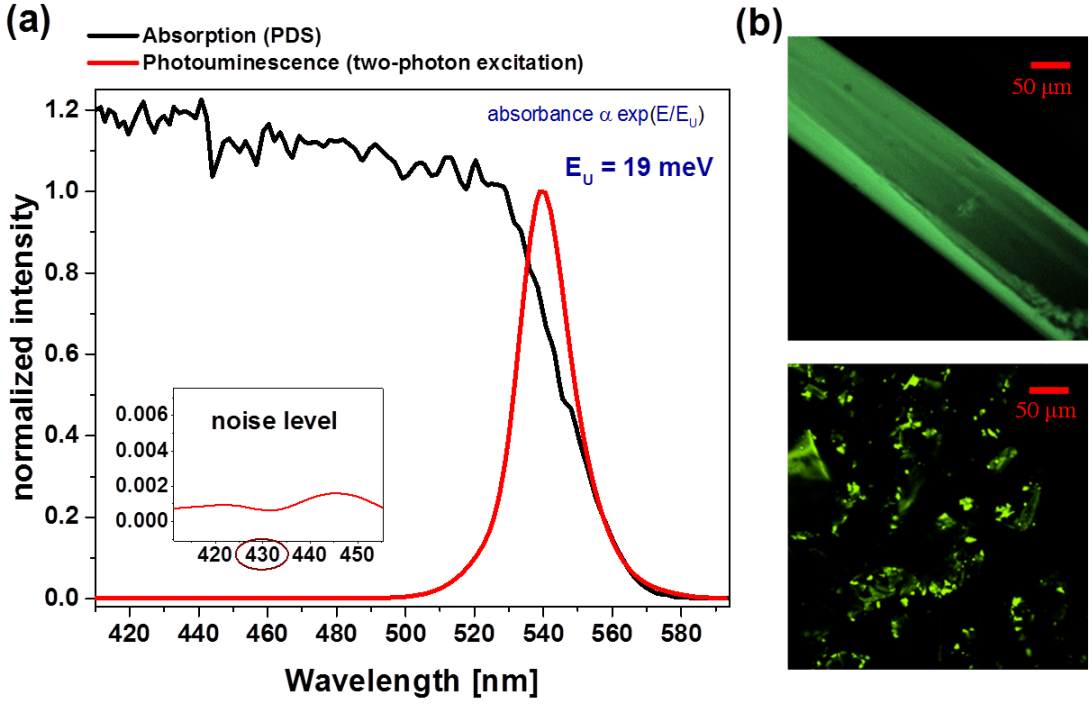

Fig. 3: (a) $CsPbBr_3$ solution-grown single crystal absorption (from PDS) and photoluminescence (using 860 nm laser) spectra. The Urbach energy is calculated from the absorbance data (*Fig. S6*). A higher resolution spectrum (inset) shows no signs of SHG at 430 nm. (b) Two 860 nm photon-excited photoluminescence images of a crystal (top) and of a dispersed powder, obtained from grinding a crystal (bottom).

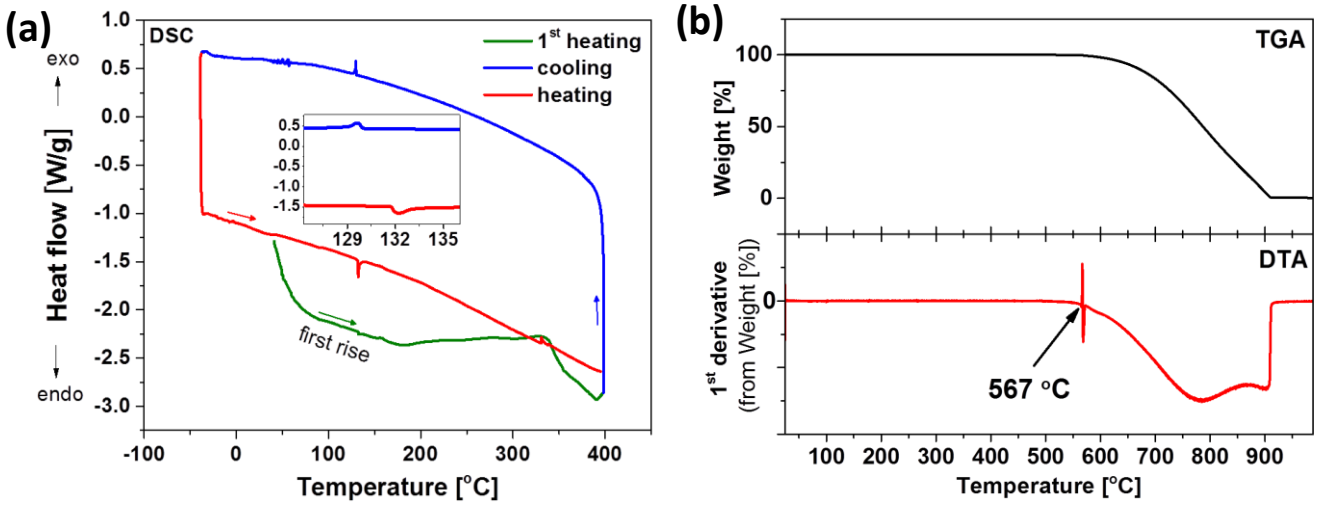

Fig. 4: (a) DSC and (b) TGA and DTA of powdered samples, obtained from pulverizing solution-grown $CsPbBr_3$ crystals. At 131 °C (inset in (a)) a phase transition between tetragonal and cubic structure occurs.[23,24] At 567 °C (differential-thermogravimetric-analysis (DTA) in (b)) the crystal melts – in agreement with literature values for melt-grown $CsPbBr_3$ crystals[7] and with results from the TGA analysis obtained from spin-coated $CsPbBr_3$.[8] The green line in (a) indicates that there is no sharp change during the first heating cycle, as sometimes occurred when a single crystal was analyzed (see *Fig. S5* and further discussion in the text).

From optical absorption data, obtained by PDS (**Fig.3** and *Fig. S6*), an Urbach energy of E_u=19 meV was derived from the slope of the logarithmic plot of the absorbance vs. the photon energy ($absorbance \propto \exp[\frac{E}{E_U}]$). While this is higher than the 15 meV value found for $MAPbI_3$, it is small compared to that of e.g., $Cu(In,Ga)Se_2$ (Table 2 in Ref. 25). We also find that a thin film that was prepared by spin coating from a similar DMSO solution shows a higher Urbach energy (~36 meV; *Fig. S6(b))*, which implies that the single crystal is of high quality. The $CsPbBr_3$ thin film fabrication procedure is reported elsewhere.[9]

Impedance spectroscopy (IS) between two parallel faces of a single crystal, using carbon-pasted contacts, was used to get the bulk resistivity and relative permittivity (**Fig. 5** and *Fig. S7*). The average resistivity, ρ, of the solution-grown crystals was found to be ~ 0.10 ± 0.04 GΩ·cm and relative permittivity $\varepsilon_r \approx$ 41 ± 4. The resistivity is an order of magnitude lower than that of crystals obtained by melt-based synthesis (~1 GΩ·cm).[7] Regarding ε_r, we find it higher than the estimated optical one ($\varepsilon_{r\ (optical)}$ ~4).[26] Similarly, the optical dielectric constants of $MAPbBr_3$ and $MAPbI_3$ are found to be ~4.5 and 6.5 [27], while their GHz (microwave) dielectric constants are ~25 and 30, respectively[20]. When illuminating (ca. 5 mW/cm^2 of a white LED) during the IS measurement, we find that the resistivity decreases by ~1 order of magnitude (**Fig. 5**). The small drop in resistivity is probably due to the opaque layer of carbon used as a contact, which shades a large fraction of the crystal (as it was deposited on the largest facets). Considering the electrode configuration and that the crystal itself is opaque to light (absorbing about ~1 μm into the crystal – see *Fig. S6*), the overall observed photoconductivity seems to be reasonable.

Two different excited carrier lifetimes were found by TRPL (**Fig.6**)): 4.4 ± 0.1 ns and 30 ± 3 ns, which are speculated to be the trap-assisted and free charge carrier recombination-based decays, respectively.[28] Both lifetime regimes are significantly shorter than those reported for $MAPbI_3$ and $MAPbBr_3$ single crystals.[10] Other fully-inorganic photovoltaic-grade materials, CIGS and CdTe show lifetimes of ~50 [29] and ~150 ns [30], respectively. In addition, a ~50 meV red-shift, which is observed in the PL decay over time, may indicate photon recycling as was recently suggested[31,32] and subsequently reported for $MAPbI_3$ [33]. An alternative reason might be diffusion and relaxation of the excited carriers to lower energy levels as the PL decays over time.

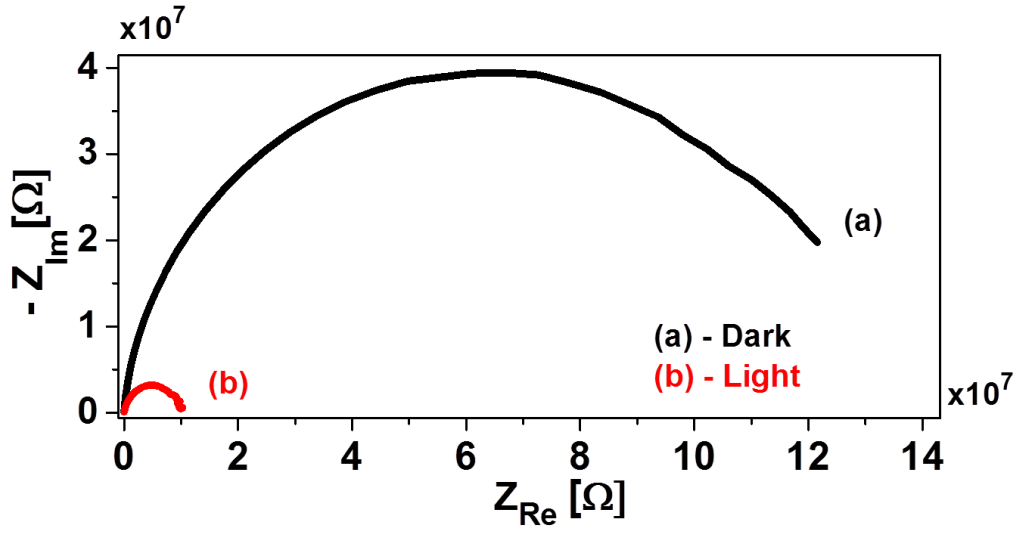

Fig. 5: IS (in air at 48% RH) between two parallel faces of a solution-grown $CsPbBr_3$ single crystal in the dark and under white LED illumination (5-7 mW/cm^2 – calibrated with a Si diode).

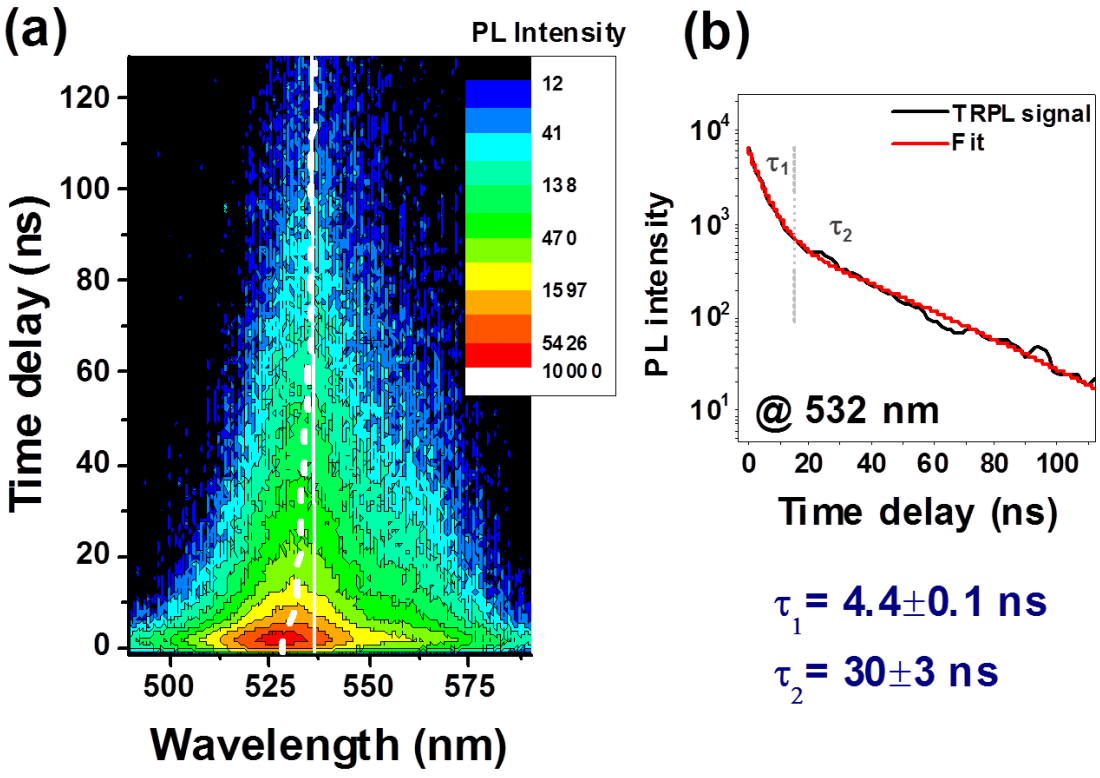

Fig. 6: TRPL spectroscopy of solution-grown $CsPbBr_3$ crystals. (a) A full PL spectrum representation with respect to time and intensity – shows that the maximum intensity shifts with time towards longer wavelength (white dashed line). (b) PL intensity vs time at 532 nm from which the short and long lifetimes are extracted. τ_1 and τ_2 are speculated to be the trap-assisted and free-charge carrier-recombination based decays, respectively.[28]

Discussion:

Crystallization process

While unraveling of the crystallization mechanism of solution-grown $CsPbBr_3$ crystals awaits further study, we draw attention to several qualitative observations.

-1- The maximum solubility of the components at room-temperature was found to be ca. 0.5 M, which was achieved only after mixing the two components. Solubility tests of $PbBr_2$ and CsBr precursors individually showed that, although 0.183 g/mL (0.50 M) $PbBr_2$ completely dissolved in DMSO (still below the solubility limit), only 0.055 g/mL (0.26 M) of CsBr could be dissolved in DMSO. The remaining 0.24 M seem to form a soluble [(x)CsBr·(y)$PbBr_2$] complex with DMSO, where (x) and (y) are stoichiometric factors. To test the effect of adding an anti-solvent to a CsBr-depleted solution, we prepared a precursor solution of 0.25 M CsBr and 0.5 M $PbBr_2$. Upon slow addition of MeCN, we found that before getting to the saturation point (where the orange precipitant stops re-dissolving) the CsBr-depleted solution stays clear, unlike the case with the equimolar solution (see *Fig. S1(a)*). This supports the existence of CsBr excess as an available species for crystallization. These examples further suggest that it is possible to find an optimal concentration balance between the precursors (which might be, as in this case, not 1:1) in which the addition of an anti-solvent will result in precipitation of a desired product. Titrating up to the saturation point of the DMSO precursor solution and further filtrating it, forced the system to get close to this optimal ratio. This method might have potential as a generic way of extracting a desired product out of similarly-challenging systems.

-2- Although finding a proper anti-solvent might seem to be a matter of luck, we noticed that among the 9 tested anti-solvents, those with the highest dielectric constants (MeCN ($\varepsilon \approx 37$), MeOH ($\varepsilon \approx 32$) and H_2O ($\varepsilon \approx 78$)) showed positive results of $CsPbBr_3$ formation, where those of MeCN and MeOH are the closest to that of DMSO (~42).[34] The solvation of ions in polar, aprotic solvents (such as DMSO) is usually *via* the first solvation shell of the ions in ion-solvent interactions[35] (i.e. complexation). The high dielectric constant, therefore, plays an important role in screening the interactions between the solvated salts and the solvent (DMSO). We noticed that addition of anti-solvents with low dielectric constant usually results in preferred precipitation of the Cs_4PbBr_6 compound. However, when the anti-solvent has a higher

dielectric constant than the solvent (compare between H_2O and DMSO), much less of the (Cs-rich) Cs_4PbBr_6 precipitates. After adding a certain amount of H_2O, a white precipitate appears (see *Fig. S3*), which is attributed (based on Ref. 23) to $CsPb_2Br_5$ ($PbBr_2$-rich) phase. This suggests that the unique precursor ratio (described in the previous point) should be coupled to a specific anti-solvent, the dielectric constant of which plays a significant role.

Crystal characterization:

The solution–based path described here is found to yield good quality $CsPbBr_3$ single crystals. Based on results from XRD, EDS, TGA and DSC, these are similar to those obtained for crystals grown at melting temperatures (> 600°C; Bridgman method). The crystals are grown in a matter of a few hours (using the HSR method) up to a few days (using the VSA method). For future studies and possible applications, the VSA method with MeCN as an anti-solvent was found to be the most suitable one, as it provides the most controllable and reproducible way of growing crystals. Nevertheless, one may find the other anti-solvents or, especially, the HSR method more appealing – mostly due to its comparative simplicity and speed of preparation.

Despite the similarity, the solution-grown crystals differ from the thermally grown ones in some respects, such as their conductivity. It is reasonable to assume that, due to the presence of a solvent and the lower temperature, the crystallization kinetics will be different and, thus, the defect density and resulting properties may be different. Therefore, apart from the simplicity, which will make such single crystals more readily accessible for research purposes or for optoelectronic uses (e.g. x-ray or γ-ray detection as was previously demonstrated[7]), crystals from low-temperature solution-based growth will likely be closer in their properties to those of solution-deposited HaP films, which are used in solar cells and LEDs.

Another issue that arises due to the use of a solution medium for crystal growth is occluded solvent molecules, which can lead to defects in the crystal. Although thermal analysis of the powder did not show clear signs of trapped solvent, similar analysis for single crystals showed features that may be attributed to trapped solvent (*Fig. S5*). More work is required to resolve this point.

For a more detailed investigation of possible distortions or defects in the solution-grown crystal, SHG and Urbach energy measurements were carried out. SHG spectroscopy showed

(Fig.3) that growth from solution does not lead to a breaking of the symmetry to a non-centrosymmetric space group (as might be the case because of defects in the crystal). Some very weak, but non-zero, SHG signal that came from a thermally-grown $CsPbBr_3$ single crystals was attributed to surface- or local defect-related symmetry breaking, a signal that was not detected in our measurements.[36] It was also found that the Urbach energy, a parameter that can be correlated with electronic disorder,[37] is only 19 meV, lower than what has been reported for photovoltaic-quality CIGS thin films.[25] Due to the crystal thickness, this value of the Urbach energy should also be taken as an upper-limit and might actually be lower (for further explanation see *Fig. S6* and 'Characterization methods' section in the *supporting information*). Still, the lower resistivity than that of melt-grown $CsPbBr_3$, the shorter lifetime than that found for other solution-grown HaP single crystals, and the ~50 meV red shift in the PL with relaxation time might indicate that further purification of the crystals may be possible.

The hybrid organic-inorganic $MAPbBr_3$ HaP shows lower long-term stability than the fully inorganic analog, but has similar mechanical properties and gives comparable photovoltaic performance.[8,9,21] The Young's modulus (15.8 ± 0.6 GPa) and hardness (~0.34 ± 0.02 GPa) of these solution-grown crystals are quite similar to those of $MAPbBr_3$ (~19.6 ± 0.03 GPa and ~0.36 ± 0.02 GPa, respectively)[21] - an indication for the lack of importance of the A group (Cs^+ vs. MA^+) in the dominating interatomic bonds. Since solution-grown $CsPbBr_3$ single crystals show photoconductivity (**Fig. 5**) and non-linear absorption (**Fig. 3(b)**), Cs can replace the organic cation to give a more reliable material for (low-cost) single crystal-related applications (e.g., photodetectors, as was demonstrated for $MAPbI_3$ [6], $MAPbCl_3$ [5] or non-linear absorbers for ultra-fast photonics, as demonstrated for $MAPbBr_3$ [38]).

Summary:

We described simple, reproducible procedures to grow high quality $CsPbBr_3$ single crystals from solution without the usually observed related byproducts: Cs_4PbBr_6 and $CsPb_2Br_5$. Two separate methods were found to be suitable: -1- slow Vapor-Saturation of an Anti-solvent (VSA) and -2- Slow Heating of a solution with a Retrograde-Soluble compound (HRS). For both methods a precursor ($PbBr_2$ and CsBr) DMSO solution was first titrated with one of the following anti-solvents: MeCN or MeOH. The pre-saturation step was important to prevent

precipitation of the undesired Cs_4PbBr_6. For the VSA method, MeCN was found to be more suitable than MeOH, while for the HRS method, MeOH is preferable.

The low temperature solution-grown method presented here provides a readily available alternative to obtain high quality, mm-size, $CsPbBr_3$ single crystals to the thermally-grown method (> 600°C). The absence of symmetry-breaking (based on SHG spectroscopy) and the 19 meV upper-limit of the Urbach energy suggest high quality of the solution-grown crystals. The dielectric constant (at sub-MHz dielectric response) was found to be ~ 40.

The order of magnitude lower resistivity, compared to thermally grown $CsPbBr_3$, and the low excited carrier lifetime, compared to other hybrid HaPs, suggest the presence of appreciable dopant (charged defect) density in the $CsPbBr_3$ crystals formed by this growth method. If true, this implies the possibility to control the crystal doping: intrinsically (by modifying the growth conditions) or extrinsically (by adding known impurities to the solution medium). The fact that $CsPbBr_3$ is clearly more stable than $MAPbBr_3$, but with similar mechanical and optoelectronic properties, suggests that the methods described in this paper may allow production of more reliable optoelectronic components, with respect to analogous hybrid HaPs.

Because high dipole moment aprotic solvents (e.g., DMSO, DMF, GBL) are commonly used in synthesis of HaPs (for both thin films and single crystals), the presented growth method is a potential path to grow perovskite structures with both organic and inorganic *A* group, similar to recently reported $Cs_{0.2}FA_{0.8}PbI_{2.84}Br_{0.16}$ thin films.[39] A combination of organic (e.g. MA and FA) and inorganic (e.g. Cs, Rb) monovalent cations may lead us to better understanding of the organic cation's role in halide perovskites. The present work is an important step towards this goal.

Acknowledgments:

The authors thank Dr. David Ehre, Arava Zohar, Dr. Isai Feldman and Dr. Thomas M. Brenner from the Weizmann Institute of Science for fruitful discussions. G.H and D.C acknowledge the Israel Ministry of Science and the Israel National Nano-Initiative for partial support. A.S., M.L.B. and R.H.F would like acknowledge EPSRC for their support. A.S. would also like to acknowledge support from an India-UK APEX project. D.C. holds the Sylvia and Rowland Schaefer Chair in Energy Research.

References:

1 P. K. Nayak and D. Cahen, *Adv. Mater.*, 2014, **26**, 1622–1628.
2 M. A. Green, K. Emery, Y. Hishikawa, W. Warta and E. D. Dunlop, *Prog. Photovolt. Res. Appl.*, 2016, **24**, 3–11.
3 A. Swarnkar, R. Chulliyil, V. K. Ravi, M. Irfanullah, A. Chowdhury and A. Nag, *Angew. Chem. Int. Ed.*, 2015, **54**, 15424–15428.
4 X. Li, Y. Wu, S. Zhang, B. Cai, Y. Gu, J. Song and H. Zeng, *Adv. Funct. Mater.*, 2016, n/a–n/a.
5 G. Maculan, A. D. Sheikh, A. L. Abdelhady, M. I. Saidaminov, M. A. Haque, B. Murali, E. Alarousu, O. F. Mohammed, T. Wu and O. M. Bakr, *J. Phys. Chem. Lett.*, 2015, **6**, 3781–3786.
6 Z. Lian, Q. Yan, Q. Lv, Y. Wang, L. Liu, L. Zhang, S. Pan, Q. Li, L. Wang and J.-L. Sun, *Sci. Rep.*, 2015, **5**, 16563.
7 C. C. Stoumpos, C. D. Malliakas, J. A. Peters, Z. Liu, M. Sebastian, J. Im, T. C. Chasapis, A. C. Wibowo, D. Y. Chung, A. J. Freeman, B. W. Wessels and M. G. Kanatzidis, *Cryst. Growth Des.*, 2013, **13**, 2722–2727.
8 M. Kulbak, S. Gupta, N. Kedem, I. Levine, T. Bendikov, G. Hodes and D. Cahen, *J. Phys. Chem. Lett.*, 2016, **7**, 167–172.
9 M. Kulbak, D. Cahen and G. Hodes, *J. Phys. Chem. Lett.*, 2015, **6**, 2452–2456.
10 D. Shi, V. Adinolfi, R. Comin, M. Yuan, E. Alarousu, A. Buin, Y. Chen, S. Hoogland, A. Rothenberger, K. Katsiev, Y. Losovyj, X. Zhang, P. A. Dowben, O. F. Mohammed, E. H. Sargent and O. M. Bakr, *Science*, 2015, **347**, 519–522.
11 Y. Tidhar, E. Edri, H. Weissman, D. Zohar, G. Hodes, D. Cahen, B. Rybtchinski and S. Kirmayer, *J. Am. Chem. Soc.*, 2014, **136**, 13249–13256.
12 Y. Liu, Z. Yang, D. Cui, X. Ren, J. Sun, X. Liu, J. Zhang, Q. Wei, H. Fan, F. Yu, X. Zhang, C. Zhao and S. F. Liu, *Adv. Mater.*, 2015, **27**, 5176–5183.
13 Y. Dang, Y. Liu, Y. Sun, D. Yuan, X. Liu, W. Lu, G. Liu, H. Xia and X. Tao, *CrystEngComm*, 2014, **17**, 665–670.
14 Y. Dang, Y. Zhou, X. Liu, D. Ju, S. Xia, H. Xia and X. Tao, *Angew. Chem. Int. Ed.*, 2016, **55**, 3447–3450.
15 C. K. Møller, *Nature*, 1958, **182**, 1436–1436.
16 M. Kobayashi, K. Omata, S. Sugimoto, Y. Tamagawa, T. Kuroiwa, H. Asada, H. Takeuchi and S. Kondo, *Nucl. Instrum. Methods Phys. Res. Sect. Accel. Spectrometers Detect. Assoc. Equip.*, 2008, **592**, 369–373.
17 M. I. Saidaminov, A. L. Abdelhady, G. Maculan and O. M. Bakr, *Chem Commun*, 2015, **51**, 17658–17661.
18 M. Cola, V. Massarotti, R. Riccardi and C. Sinistri, *Z. Für Naturforschung A*, 1971, **26**, 1328.
19 N. Yantara, S. Bhaumik, F. Yan, D. Sabba, H. A. Dewi, N. Mathews, P. P. Boix, H. V. Demir and S. Mhaisalkar, *J. Phys. Chem. Lett.*, 2015, **6**, 4360–4364.
20 M. I. Saidaminov, A. L. Abdelhady, B. Murali, E. Alarousu, V. M. Burlakov, W. Peng, I. Dursun, L. Wang, Y. He, G. Maculan, A. Goriely, T. Wu, O. F. Mohammed and O. M. Bakr, *Nat. Commun.*, 2015, **6**, 7586.
21 Y. Rakita, S. R. Cohen, N. K. Kedem, G. Hodes and D. Cahen, *MRS Commun.*, 2015, **5**, 623–629.
22 R. W. Boyd, *Nonlinear optics*, Elsevier/Academic Press, Amsterdam, 3. ed., 2008.
23 M. Rodová, J. Brožek, K. Knížek and K. Nitsch, *J. Therm. Anal. Calorim.*, 2003, **71**, 667–673.
24 S. Hirotsu, J. Harada, M. Iizumi and K. Gesi, *J. Phys. Soc. Jpn.*, 1974, **37**, 1393–1398.
25 S. D. Stranks and H. J. Snaith, *Nat. Nanotechnol.*, 2015, **10**, 391–402.
26 D. Sapori, M. Kepenekian, L. Pedesseau, C. Katan and J. Even, *Nanoscale*, 2016, **8**, 6369–6378.
27 K. Tanaka, T. Takahashi, T. Ban, T. Kondo, K. Uchida and N. Miura, *Solid State Commun.*, 2003, **127**, 619–623.
28 F. Deschler, M. Price, S. Pathak, L. E. Klintberg, D.-D. Jarausch, R. Higler, S. Hüttner, T. Leijtens, S. D. Stranks, H. J. Snaith, M. Atatüre, R. T. Phillips and R. H. Friend, *J. Phys. Chem. Lett.*, 2014, **5**, 1421–1426.
29 I. L. Repins, W. K. Metzger, C. L. Perkins, J. V. Li and M. A. Contreras, *IEEE Trans. Electron Devices*, 2010, **57**, 2957–2963.
30 S. Johnston, K. Zaunbrecher, R. Ahrenkiel, D. Kuciauskas, D. Albin and W. Metzger, *IEEE J. Photovolt.*, 2014, **4**, 1295–1300.
31 G. Hodes and P. V. Kamat, *J. Phys. Chem. Lett.*, 2015, **6**, 4090–4092.
32 W. E. I. Sha, X. Ren, L. Chen and W. C. H. Choy, *Appl. Phys. Lett.*, 2015, **106**, 221104.
33 L. M. Pazos-Outon, M. Szumilo, R. Lamboll, J. M. Richter, M. Crespo-Quesada, M. Abdi-Jalebi, H. J. Beeson, M. Vru ini, M. Alsari, H. J. Snaith, B. Ehrler, R. H. Friend and F. Deschler, *Science*, 2016, **351**, 1430–1433.
34 W. M. Haynes, CRC handbook of chemistry and physics. CRC press, London 2014.
35 H. Inerowicz and E. Kamienska-Piotrowicz, *Thermochim. Acta*, 1989, **145**, 219–226.

36 D. J. Clark, C. C. Stoumpos, F. O. Saouma, M. G. Kanatzidis and J. I. Jang, *Phys. Rev. B*, 2016, **93**, 195202.
37 J. I. Pankove, Optical Processes in Semiconductors, chapter 3, Dover Publications, New York 1971.
38 G. Walters, B. R. Sutherland, S. Hoogland, D. Shi, R. Comin, D. P. Sellan, O. M. Bakr and E. H. Sargent, *ACS Nano*, 2015, **9**, 9340–9346.
39 C. Yi, J. Luo, S. Meloni, A. Boziki, N. Ashari-Astani, C. Grätzel, S. M. Zakeeruddin, U. Röthlisberger and M. Grätzel, *Energy Environ. Sci.*, 2016, **9**, 656–662.

Supplementary Information

Low-Temperature Solution Grown $CsPbBr_3$ Single-Crystals and Their Characterization

Yevgeny Rakita[a], Nir Kedem[a], Satyajit Gupta[a], Aditya Sadhanala[b], Vyacheslav Kalchenko[c], Marcus L. Böhm[b], Michael Kulbak[a], Richard H. Friend[b], David Cahen[a]* and Gary Hodes[a]*

a. *Materials and Interfaces Department, Weizmann Institute of Science, Rehovot, 7610001, Israel*
b. *Cavendish Laboratory, JJ Thomson Avenue, Cambridge CB3 0HE, United Kingdom*
c. *Veterinary Resources Departments; Weizmann Institute of Science, Rehovot, 7610001, Israel*

* Corresponding authors: David Cahen: david.cahen@weizmann.ac.il ; Gary Hodes: gary.hodes@weizmann.ac.il

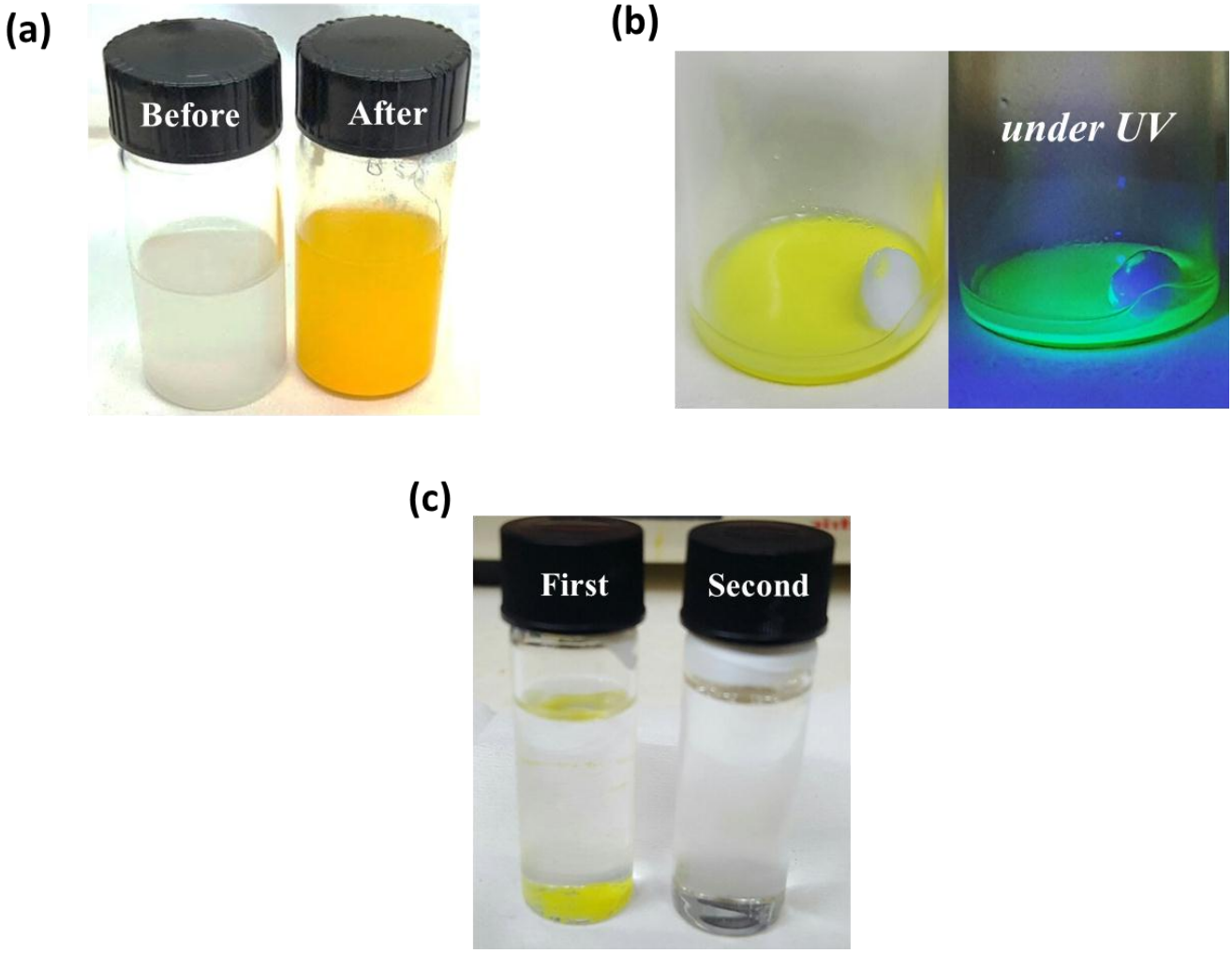

Fig. S1: (a) Unfiltered solutions just before (white-cloudy) and after (yellow-cloudy) saturation with MeCN. (b) Precipitated residuals after filtering a MeCN-saturated solution, which was heated to 50 °C under continuous stirring for 24 hours. The right picture is the same as the left one, but under UV light (365 nm), showing the strong florescent nature of the precipitate. (c) MeOH-saturated solution after the first and second heating-cooling cycles.

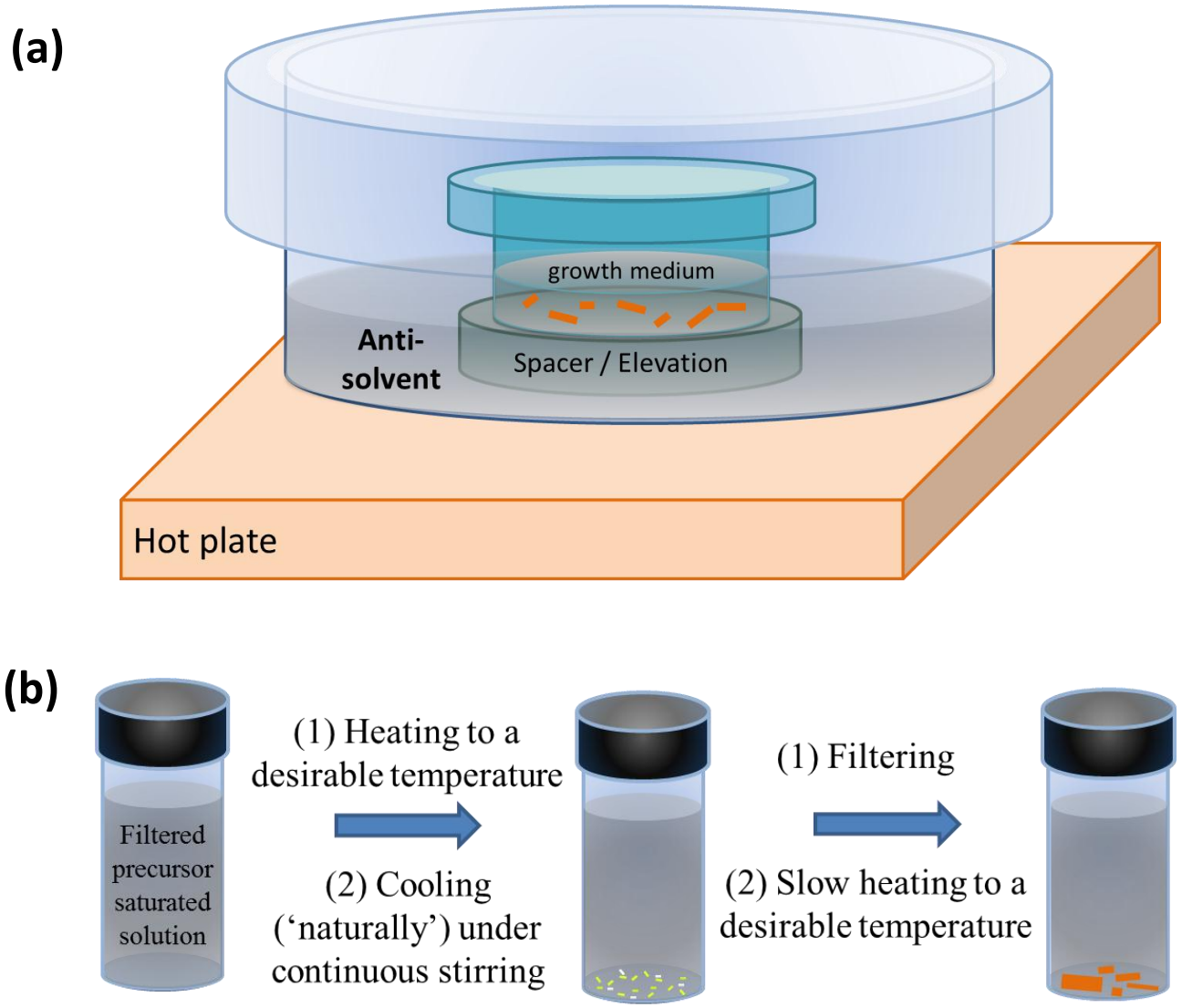

Fig. S2: (a) Schematic view of the VSA crystal growth setup. (b) Schematic view of the HRS crystal growth setup and sequence.

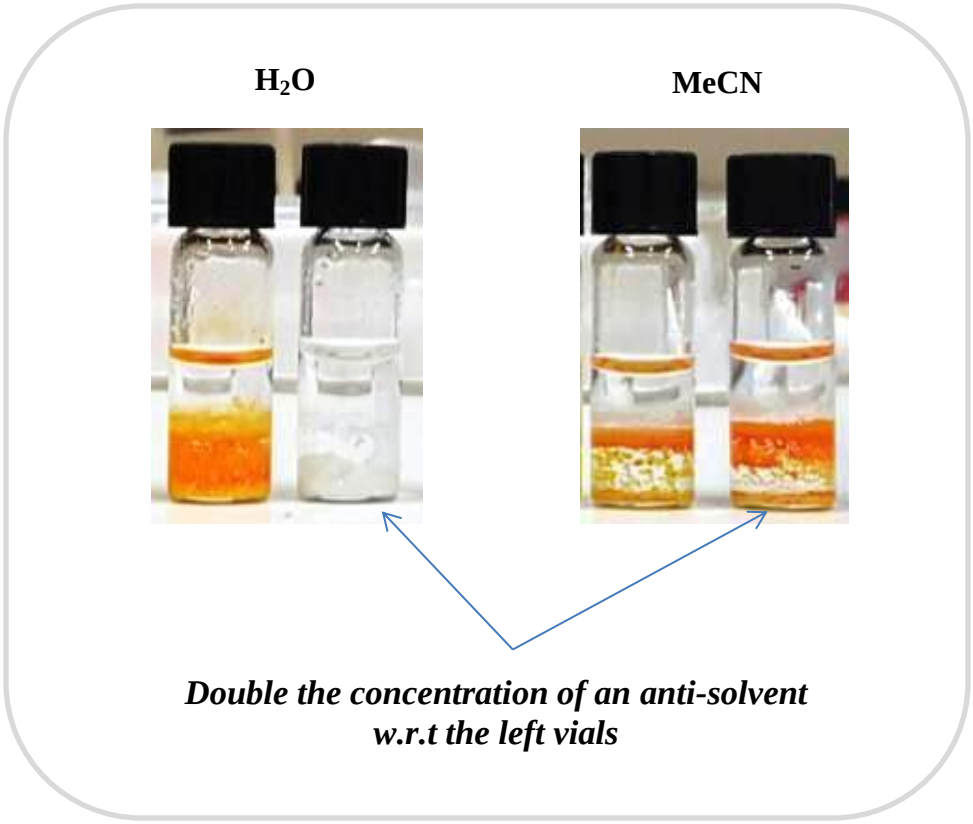

Fig. S3: Result of adding (dropwise) H_2O and MeCN as anti-solvents to 0.45 M equimolar solution of CsBr and $PbBr_2$ in DMSO. Based on M. Rodová et al[1], the colorless precipitate that was formed when we added extra water (right vial in the left pair of vials), most likely, contains the $PbBr_2$-rich phase, $CsPb_2Br_5$. It was not further investigated, as this product was not the focus of the present work. The results show that, unlike MeCN, using water as an anti-solvent will add complexity to crystal growth as the water amount has to be strictly regulated, which will limit the crystal size and, most likely, quality. Adding an excess of MeCN (not shown) does not cause further reaction.

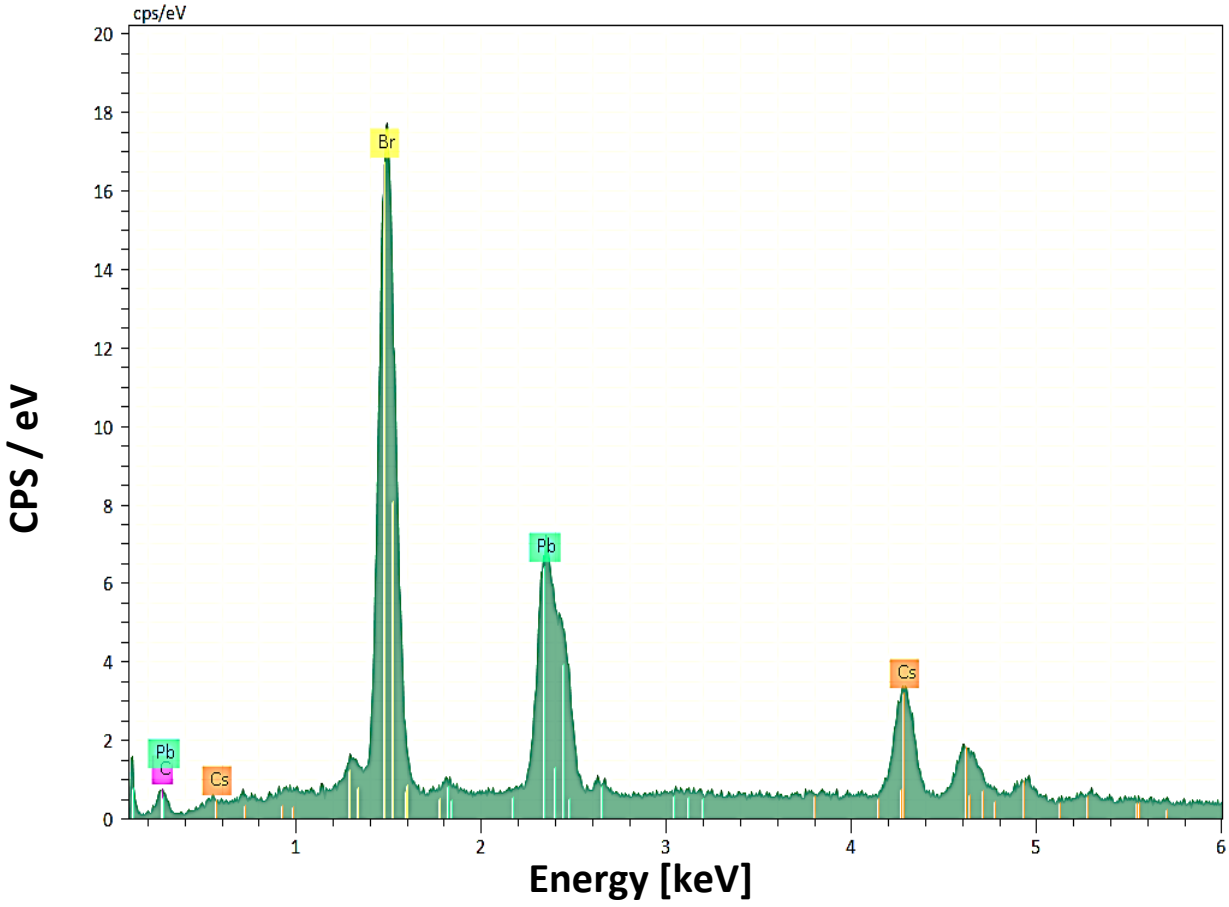

Fig. S4: EDS spectrum of a $CsPbBr_3$ single crystal. Excitation voltage was 15 keV. Elemental analysis (based on the deconvoluted peaks) between Br:Pb:Cs showed an atomic ratio of (3.4±0.1):(1):(1). Based on ref. [2], there should not be beam damage during measurements. To double check the e-beam influence on the EDS reading, we scanned the same area twice. Within the error of the measurement – the two scans showed similar results.

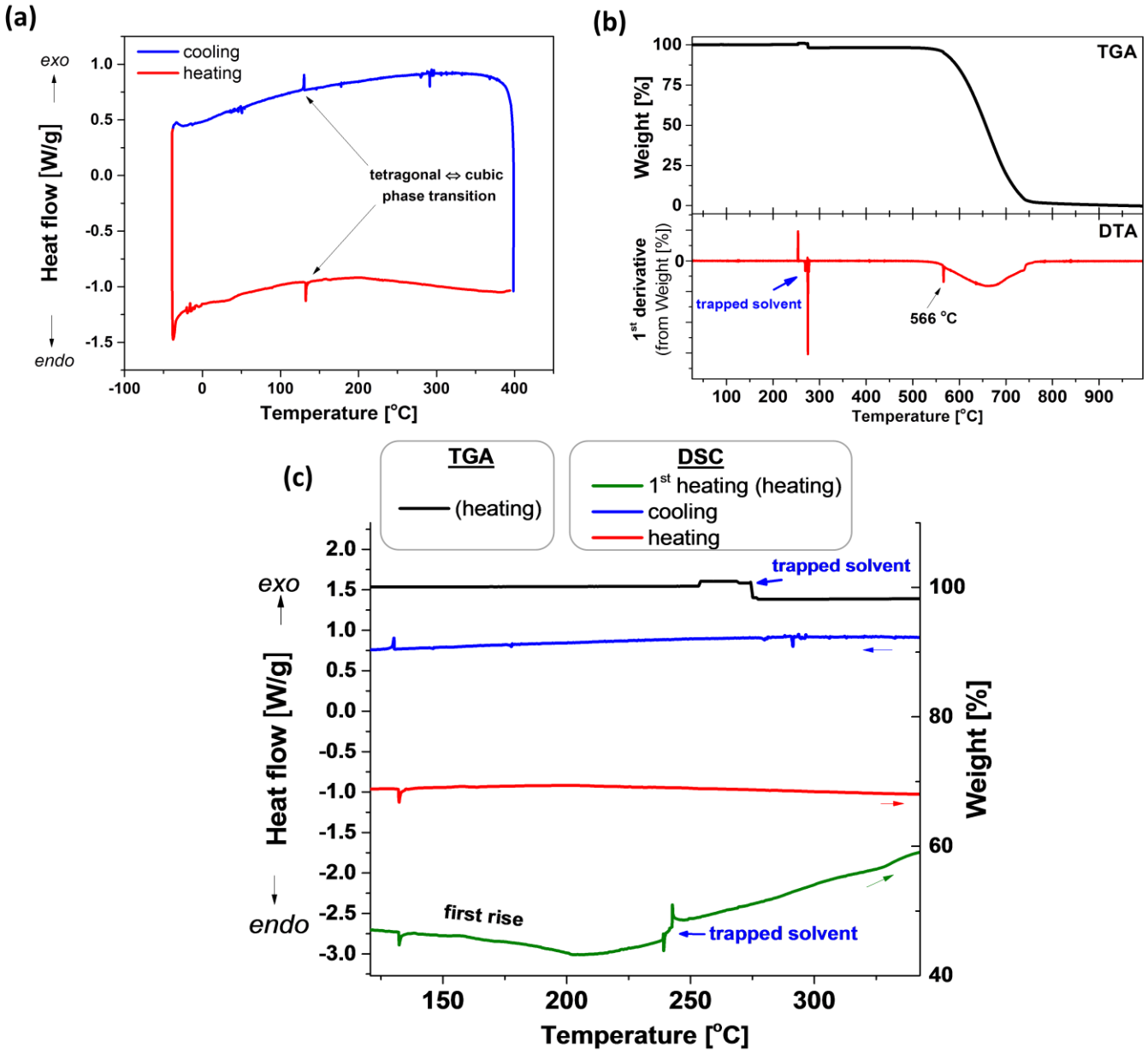

Fig. S5: (a) DSC and (b) TGA and its 1st derivative of ~0.5mm solution-grown $CsPbBr_3$ single crystals. (c) A zoom-in to an area of interest in a case where a one-time sharp change at ~230°C was evident - plausibly due to escape of occluded solvent (DMSO, bp:189°C).

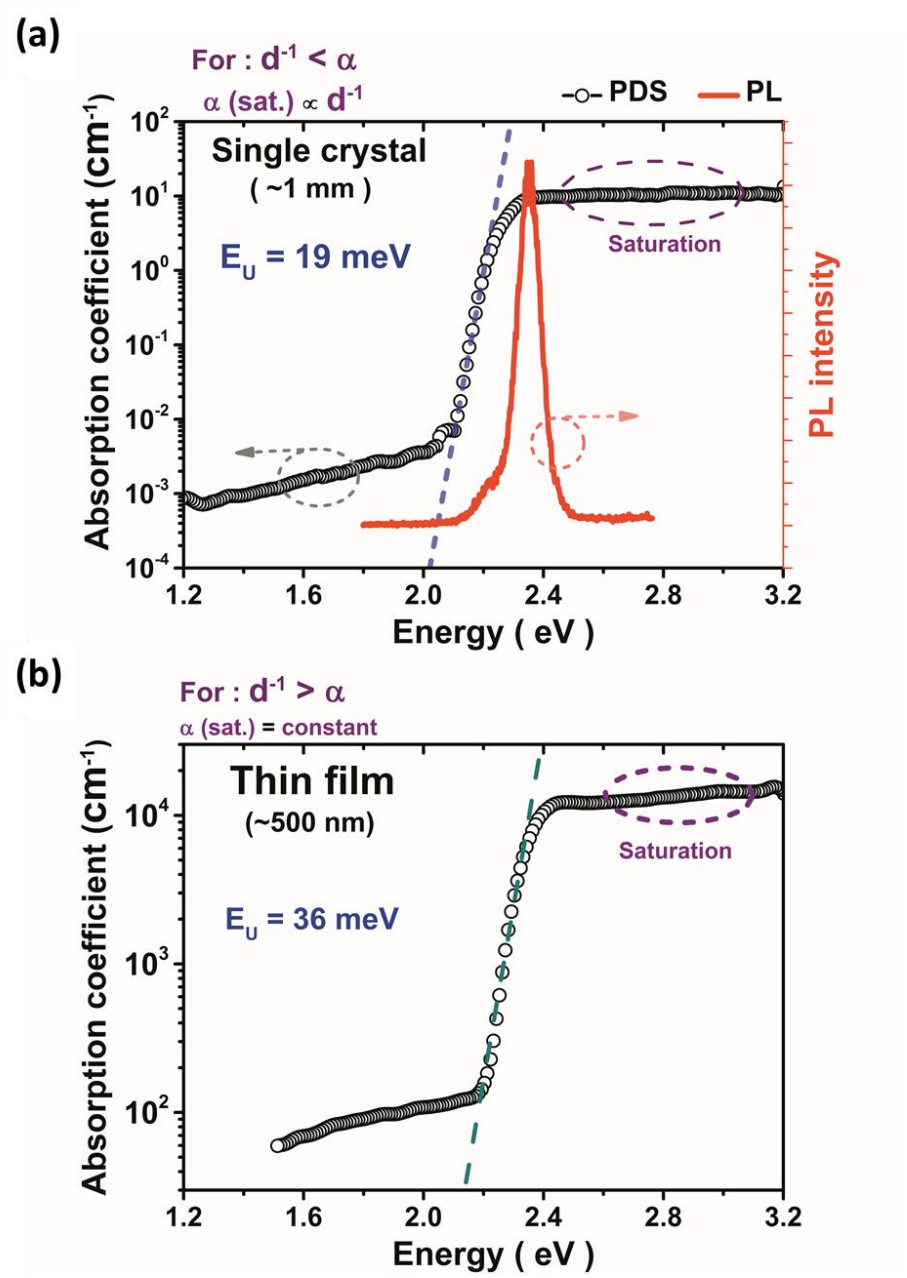

Fig. S6: Optical absorbance (plotted on a log scale) vs. the excitation energy measured by PDS of (a) a solution grown $CsPbBr_3$ crystal and (b) a spin-coated $CsPbBr_3$ thin film[3]. The red plot in (a) is a (normalized) PL spectrum of the crystal. The Urbach energy (E_U) was derived based on $\alpha \propto \exp[E/E_U]$, which is the inverse of the dashed linear fits. We see that the saturation of the PDS detector goes with one over the thickness, which is when the inverse of the probed thickness is greater than the band-to-band transition absorption coefficient (based on (b): $[\frac{1}{1.5\cdot 10^4} cm \sim$ **0.7µm**]). Hence, in a ~1 mm single crystal the penetration depth of light limits the absorbance (above 2.2eV) and, therefore, it will be featureless and flat (above 2.2eV). For further explanation about the PDS measurement, see below.

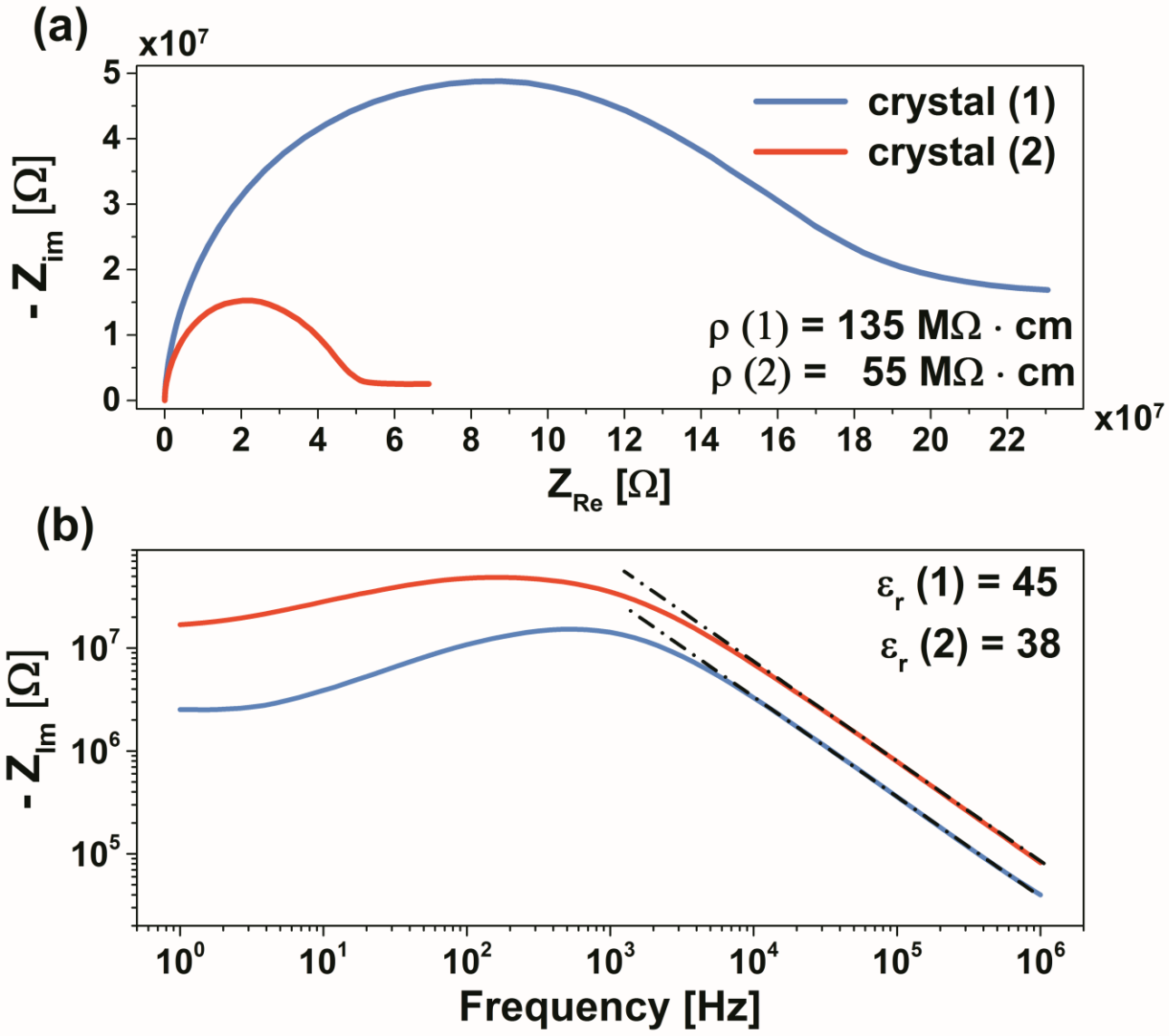

Fig. S7: IS of two single crystals. (a) is used for calculations of the resistivity and (b) for the calculations of the dielectric constant. The crystal and electrode dimensions that were used for the calculations were: crystal #(1) - $A_{(1)}$=7.8 mm^2, $d_{(1)}$ =1.0 mm ; crystals #(2) - $A_{(2)}$=6.8 mm^2, $d_{(2)}$= 0.5 mm. Calculations of resistivity and dielectric constant based on IS are described below in (look in 'Characterization methods and equipment'). The low-frequency part in (a) (higher Z_{Re} values) was not further analyzed and requires investigation to understand its origin.

Characterization methods and equipment:

- *Powder x-ray diffraction*: The X-ray analysis was done with an Ultima-III (sealed X-ray tube, Cu anode, 3 kW, RIGAKU, Japan) diffractometer using a Bragg Brentano geometry.

- *Energy-dispersive X-ray spectroscopy*: the measurements were carried out in a Zeiss (Leo, Supra) scanning electron microscope under electron beam excitation energy of 15 keV. The EDS detector was a Peltier-cooled Bruker (XFlash 6 | 60) detector with Spectral resolutions of 126 eV (calibrated for FWHM of Mn).

- *Thermal analysis*: TGA and DSC were done with a Q600 and Q200 models from "TA instruments", respectively. The TGA was carried-out in an alumina crucible under N_2 flow at a heating rate of 20 °C/min. The DSC was carried out using a hermetically sealed aluminum pans under N_2 flow at heating rate of 10 °C/min and cooling rate of 5 °C/min.

- *Second Harmonic Generation spectroscopy:* We used an LSM 880 upright system (Zeiss, Germany) with non-linear optics (NLO), coupled with a Chameleon MPX (Coherent Inc., CA, USA) femtosecond pulsed, tunable Ti : sapphire laser for two-photon excitation, with a standard, spectral (Lambda mode) acquisition with 4.4 nm steps at excitation wavelength 860 nm. Spectral analyses were performed using ZEN Imaging software from Zeiss.

- *Photothermal deflection spectroscopy (PDS)*: PDS is a scatter-free surface sensitive optical absorption measurement, capable of measuring absorbance that is 5-6 orders of magnitude weaker than the supra-band edge absorption. For the measurements, a monochromatic light beam (pump) illuminates the sample (film on quartz substrate), which upon optical absorption produces a thermal gradient near the sample surface via non-radiative relaxation-induced heating. This results in a refractive index gradient in the area surrounding the sample surface. This refractive index gradient is further enhanced by immersing the sample in an inert liquid FC-72 Fluorinert® (3M Company)

which has a high refractive index change per unit change in temperature. A fixed wavelength CW laser Probe beam is passed through this refractive index gradient producing a deflection proportional to the absorbed light at that particular wavelength, which is detected by a photo-diode and lock-in amplifier combination. Here we measure single crystals (~1 mm), that are much thicker than the optical penetration depth (~500 nm for ~2.3 eV photons) as measured for the $CsPbBr_3$ thin-film shown in *Figure S6(b)*. Therefore, PDS is not capable of probing the exact band edge of the single crystal due to the thickness being much higher than the optical penetration depth for absorption above the band edge. Normally in thin films, for obtaining the Urbach energy, one should fit the Urbach tail (or the exponential decay in the absorption below the band-edge). [4] For a single crystal that is orders of magnitude thicker than a thin film, we are more likely to see absorption from states, which have a very low density, such as deep states. Previous works have shown that the DOS of deep states is likely to exhibit a slower decay than a typical Urbach tail.[5,6] This will result in estimation of the Urbach energy being an upper limit.

- *Impedance spectroscopy:* For impedance spectroscopy analysis an Alpha-A impedance analyzer (Novocontrol Tech., Germany) was used. Measurements were carried-out at 0.1 V_{AC}. To determine the resistivity (ρ) we fit to a simple RC equivalent circuit. To find the relative permittivity (ε_r) we used the simple capacitor relation at high frequencies $C_{(\omega\to\infty)} = C_0 \cdot \varepsilon_r = \frac{1}{2\pi f \cdot Z_{Im}}$, which can be reorganized to: $\log(Z_{Im}) = -\log(f) - \log(2\pi C_0 \varepsilon_r)$. $C_0 = \varepsilon_0 \frac{A}{d}$, A is the contact area, d is the distance between the electrodes, ε_0 is the permittivity of vacuum, Z_{Im} is the imaginary impedance and f is the frequency. Then we extract ε_r from the intercept of a linear fit at the high frequency region in a $\log(Z_{Im})\ vs\ \log(f)$ plot (after making sure the slope of the linear fit is ~ (-1)).

- *Time-resolved photoluminescence*: Measurements were taken with a gated intensified CCD camera system (Andor iStar DH740 CCI-010) connected to a grating spectrometer (Andor SR303i). Excitation was performed with femtosecond laser pulses which were

generated by in a homebuilt setup by second harmonic generation (SHG) in a β-barium borate (BBO) crystal form the fundamental output (pulse energy 1.55 eV, pulse length 50 fs) of a Ti:sapphire laser system (Spectra Physics Soltstice). The laser pulses generated from the SHG had photon energy of 3.1 eV, pulse length ~100 fs and fluence 2 $\mu J/cm^2$. Temporal resolution of the PL emission was obtained by measuring the PL from the sample by stepping the iCCD gate delay for different delays with respect to the excitation. The typical gate width was 1.5 ns. Time-integrated steady state spectra were obtained by temporally averaging the emission in the detection software (exposure time 0.2 s, 5 μs gate width)

List of different anti-solvents that were used:

- H_2O – Double distilled water – purified (Millipore) to a resistance of 18.2 MΩ
- Acetone – 99.8 %, AR-b, Bio-lab LTD
- 2-propanol – 99.8 %, AR-b, Bio-lab LTD
- Ethyl acetate – 99.8 %, AR-b, Bio-lab LTD
- Tetrahydrofuran – 99.9 %, HPLC grade, Sigma-Aldrich
- Dibromomethan – 99 %, Sigma-Aldrich
- Dibromoethane – 98 %, Sigma-Aldrich

References:

1 M. Rodová, J. Brožek, K. Knížek and K. Nitsch, *J. Therm. Anal. Calorim.*, 2003, **71**, 667–673.
2 M. Kulbak, S. Gupta, N. Kedem, I. Levine, T. Bendikov, G. Hodes and D. Cahen, *J. Phys. Chem. Lett.*, 2016, **7**, 167–172.
3 M. Kulbak, D. Cahen and G. Hodes, *J. Phys. Chem. Lett.*, 2015, **6**, 2452–2456.
4 J. I. Pankove, *Optical Processes in Semiconductors*, Courier Corporation, 1971.
5 E. F. Schubert, *Light-Emitting Diodes*, Cambridge University Press, 2003.
6 M. Stella, PhD thesis, Universitat de Barcelona, 2010.

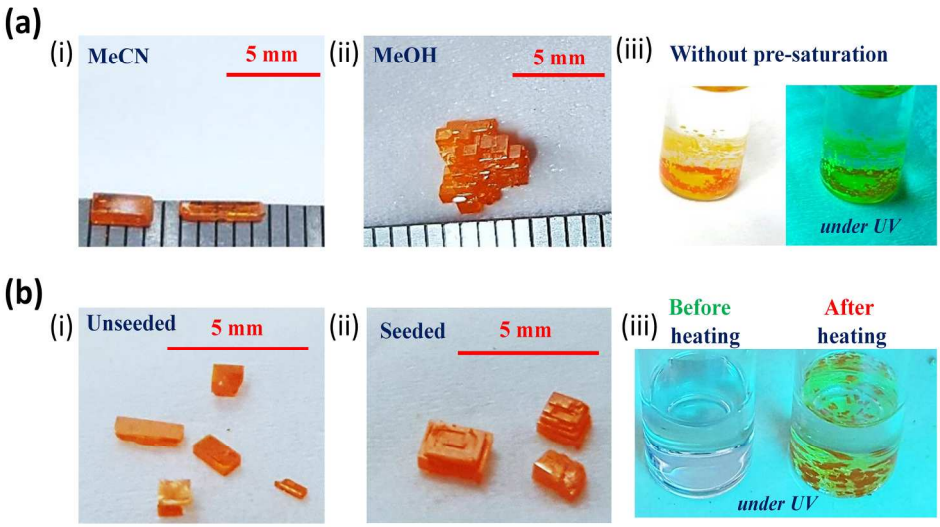

(a) $CsPbBr_3$ crystals grown by a VSA method: (i) growth from MeCN-saturated solution on a 50ºC hot-plate ; (ii) growth from MeOH-saturated solutions at RT. Both were grown for ca. 48 hours; (iii) growth from an unsaturated DMSO precursor solution, using MeCN as an anti-solvent – showing (LEFT) a yellow precipitate on top of which grew orange $CsPbBr_3$. When illuminating with a UV light (RIGHT) the yellow precipitate shows a strong green fluorescence, indicating that it contains the CsBr-rich (Cs_4PbBr_6) compound. (b) $CsPbBr_3$ crystals grown by an HRS method: growth at a heating rate of 10°C/hour up to 80°C (i) without and (ii) with seeding of freshly-grown single crystals; (iii) before and after heating to 80 °C for the first time (i.e., without a preliminary heating/cooling cycle), showing the undesired Cs_4PbBr_6 fluorescent compound as a side product.
208x159mm (300 x 300 DPI)

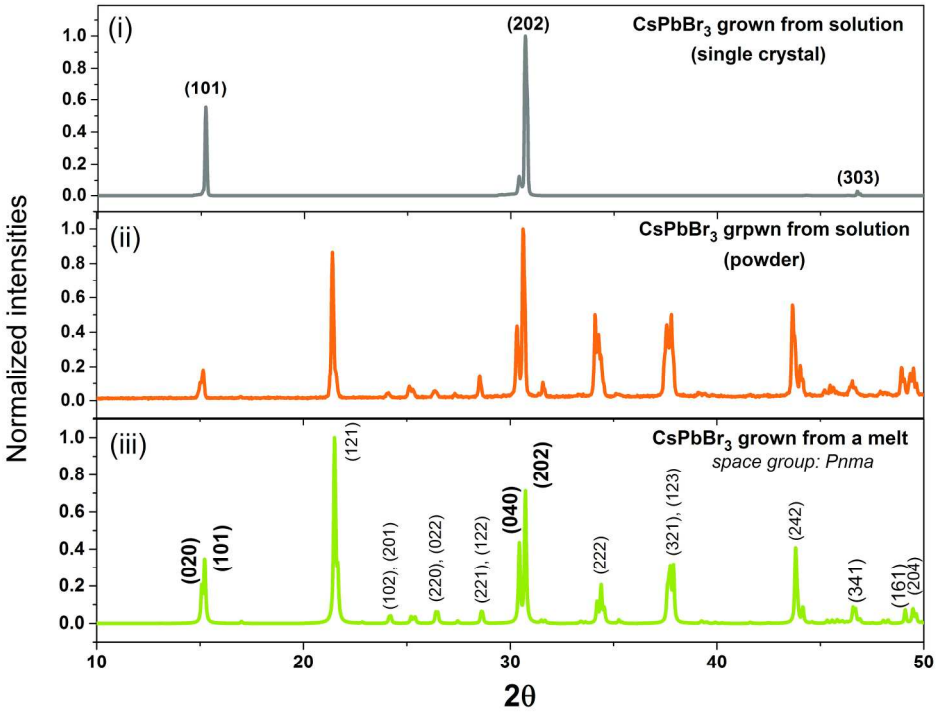

Room-temperature x-ray diffraction pattern of (i) solution-grown $CsPbBr_3$ single crystal. The natively-grown face of which was parallel to the scanning plane in a θ/2θ scan; (ii) powder scan of a pulverized solution-grown single crystal and (iii) a simulated spectrum based on thermally-grown crystals' CIF.[7] The crystal orientations written in **bold** correspond to the natively-exposed faces of the solution-grown crystal.
208x159mm (300 x 300 DPI)

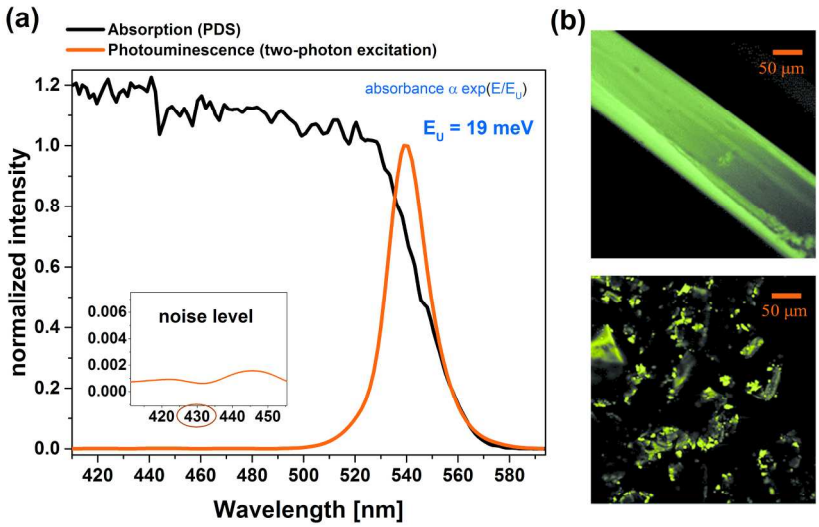

(a) $CsPbBr_3$ solution-grown single crystal absorption (from PDS) and photoluminescence (using 860 nm laser) spectra. The Urbach energy is calculated from the absorbance data (Fig. S6). A higher resolution spectrum (inset) shows no signs of SHG at 430 nm. (b) Two 860 nm photon-excited photoluminescence images of a crystal (top) and of a dispersed powder, obtained from grinding a crystal (bottom).
208x159mm (300 x 300 DPI)

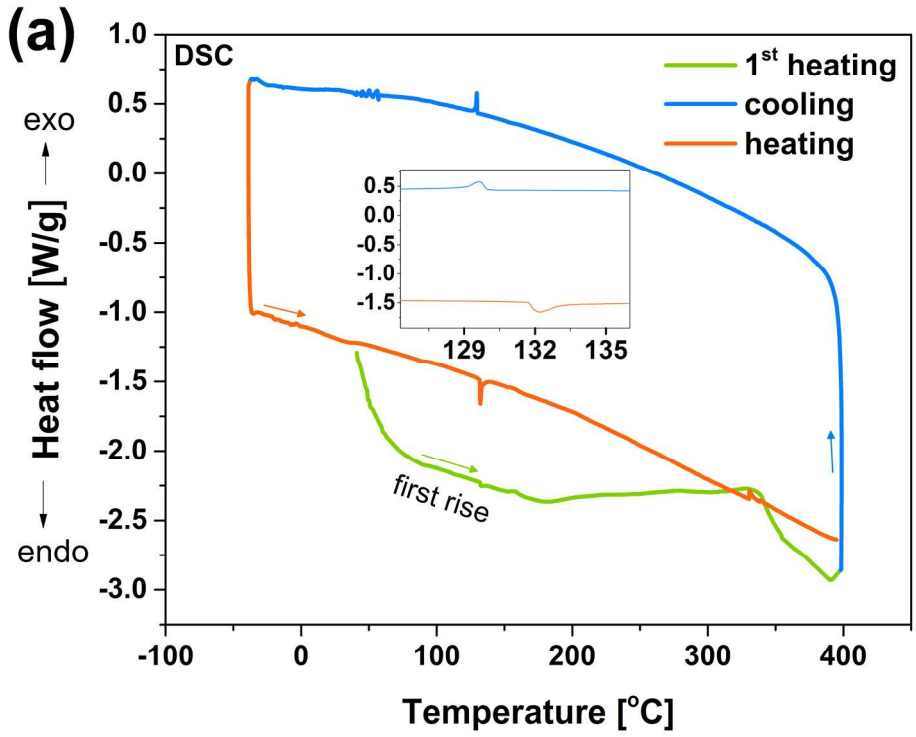

(a) DSC and (b) TGA and DTA of powdered samples, obtained from pulverizing solution-grown $CsPbBr_3$ crystals. At 131 °C (inset in (a)) a phase transition between tetragonal and cubic structure occurs.[23,24] At 567 °C (differential-thermogravimetric-analysis (DTA) in (b)) the crystal melts – in agreement with literature values for melt-grown $CsPbBr_3$ crystals[7] and with results from the TGA analysis obtained from spin-coated $CsPbBr_3$.[8] The green line in (a) indicates that there is no sharp change during the first heating cycle, as sometimes occurred when a single crystal was analyzed (see Fig. S5 and further discussion in the text).
208x159mm (300 x 300 DPI)

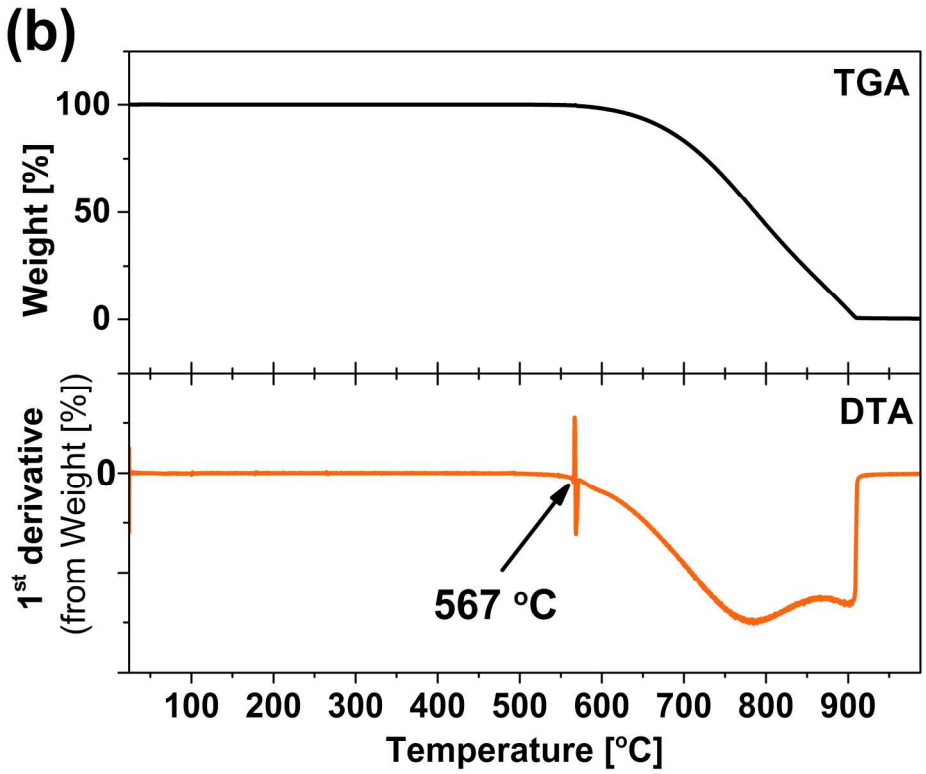

(a) DSC and (b) TGA and DTA of powdered samples, obtained from pulverizing solution-grown $CsPbBr_3$ crystals. At 131 °C (inset in (a)) a phase transition between tetragonal and cubic structure occurs.[23,24] At 567 °C (differential-thermogravimetric-analysis (DTA) in (b)) the crystal melts – in agreement with literature values for melt-grown $CsPbBr_3$ crystals[7] and with results from the TGA analysis obtained from spin-coated $CsPbBr_3$.[8] The green line in (a) indicates that there is no sharp change during the first heating cycle, as sometimes occurred when a single crystal was analyzed (see Fig. S5 and further discussion in the text).
208x159mm (300 x 300 DPI)

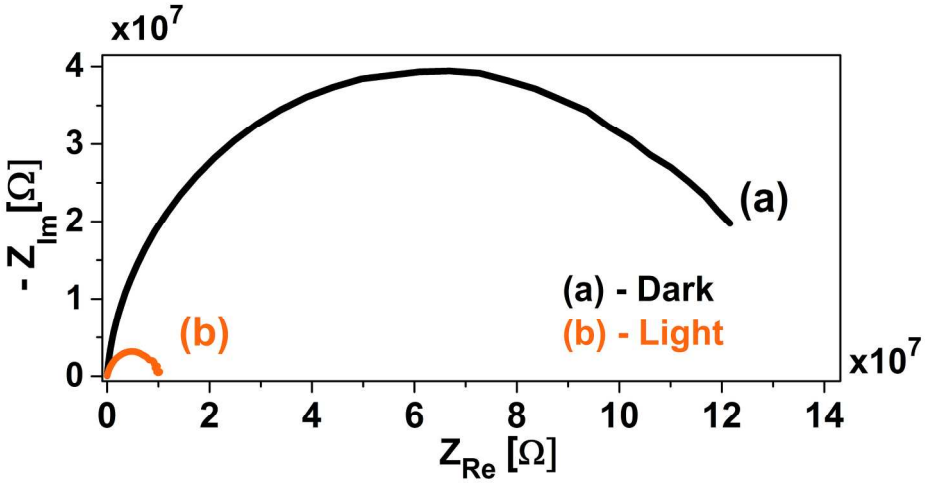

IS (in air at 48% RH) between two parallel faces of a solution-grown $CsPbBr_3$ single crystal in the dark and under white LED illumination (5-7 mW/cm^2 – calibrated with a Si diode).
208x159mm (300 x 300 DPI)

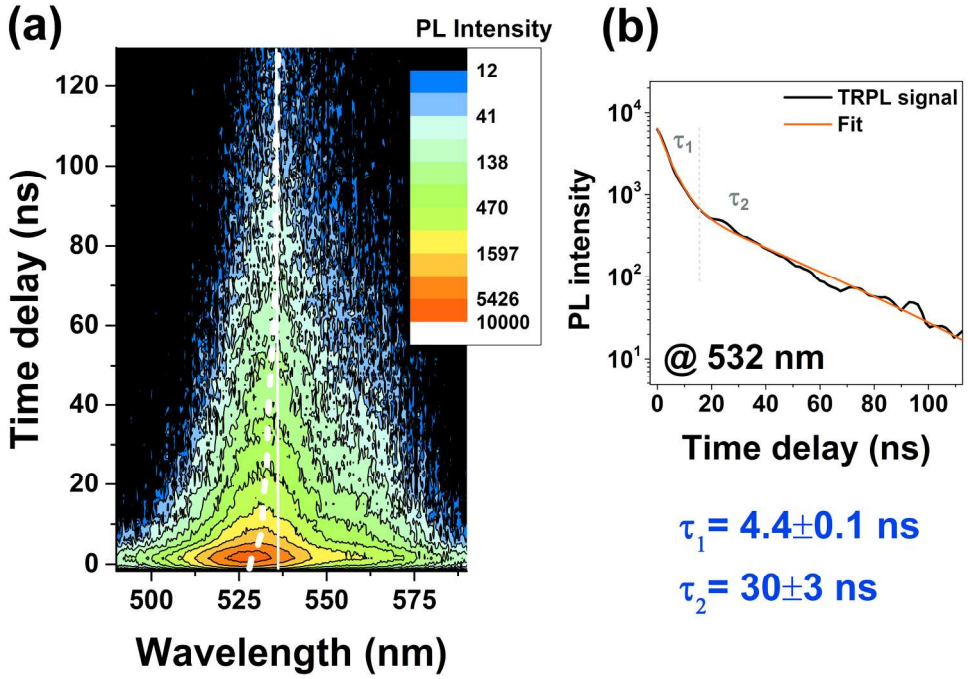

TRPL spectroscopy of solution-grown $CsPbBr_3$ crystals. (a) A full PL spectrum representation with respect to time and intensity – shows that the maximum intensity shifts with time towards longer wavelength (white dashed line). (b) PL intensity vs time at 532 nm from which the short and long lifetimes are extracted. τ_1 and τ_2 are speculated to be the trap-assisted and free-charge carrier-recombination based decays, respectively.[28]
202x141mm (300 x 300 DPI)